Ancient TL

June 2025, Volume 43, No. 1

Ancient TL

Started by the late David Zimmerman in 1977

EDITOR

Christoph Schmidt, Institute of Earth Surface Dynamics, University of Lausanne, Switzerland,
Tel: +41-21-692-3516 (christoph.schmidt@unil.ch)

EDITORIAL BOARD

ADVISORY BOARD

Web coordinators: Christoph Schmidt, Thomas Henkel
Article layout and typesetting: Christoph Schmidt
Bibliography: Christoph Schmidt

Ancient TL

Research Article

A simple activity to teach 4th–8th graders about OSL dating and its applications

Regina DeWitt[1]*

[1]Department of Physics, East Carolina University, 1000 E. 5th Street, Greenville, NC, 27858, USA

*Corresponding author: dewittr@ecu.edu

Abstract

I have developed a simple hands-on activity for 4th–8th grade children (10–14 years old), with the goal to teach about the need for geochronology and the basic principles of OSL dating. The children are first introduced to the basic concepts of OSL dating, and participate afterwards in an activity to answer a scientific question. In our case they are asked to answer the question "Do islands move?". In the hands-on part of the activity, children playfully simulate the process of dating a sample. They use measuring spoons to fill clear plastic cups with beads to a pre-determined fill level. By counting the number of spoon-loads needed, students can determine the "age" of the sample. Ages are entered into a map and the results are discussed. The activity has been designed to be suitable for varying group sizes and different settings. It can easily be adopted by other researchers, we recommend however that the scientific question be modified to fit the regional setting of each laboratory. This manuscript describes the different stages of the outreach event – i.e., introduction, hands-on activity and discussion – and the rationale behind each step, as well as the materials needed.

Keywords: Outreach activity, Science communication, Didactics

1. Introduction

In an era where scientific misinformation is rampant and public trust in science is often eroded, it has become crucially important to bridge the gap between complex scientific knowledge and the public. It is particularly important to reach out to school children, many of whom have never met a scientist in person. Their idea of a scientist is formed by TV and movies, where scientists are portrayed either as brilliant miracle-workers, who conjure up problem solutions completely out of the blue, or alternatively as social oddballs who use complex jargon and are mostly good for a laugh. To dispel these myths, we need to allow school children to come to our labs, introduce them to our every-day work, and explain how we interpret data to learn about the world around us. We need to help them build trust in science and encourage their participation in science.

For this reason, my lab, just like many others, is increasingly participating in outreach events for school children, some as young as elementary school. School classes come to visit our university, or we visit schools. The target age range of the children – in this manuscript also referred to as "students" – is 4th–8th graders, i.e., $\sim$10–14 years. These younger children do not have the attention span to enjoy a lengthy guided tour or to listen to a presentation. They are looking for hands-on activities. The purpose of the project presented in this manuscript was to develop a hands-on activity for 4th–8th graders to teach about luminescence dating and its applications. Basic requirements were: (i) The activity must be age appropriate; (ii) it must accommodate groups of up to 50 children; (iii) the whole event should take less than an hour. The development of the activity was predominantly based on experience and interactions with children. However, in many ways it follows the strategies of active learning (e.g., Edwards, 2015). The hands-on aspect ensures that the children are actively involved and have the opportunity for playful learning in a group setting. The activity builds on prior knowledge and uses real-world connections. Last but not least, an aha-moment at the end is intended to reinforce the experience (e.g., Pilcher, 2015).

The primary objective of the learning activity was for the children to gain a basic understanding of the purpose

of geochronology and how results are interpreted. The secondary goal was to introduce luminescence dating as an example of a geochronological method. To best familiarize and engage the students with the material, I considered our geographic location on the East Coast of the United States, close to the Atlantic Ocean. The activity centers on the surprising question "Do islands move?".

In the hands-on part of the activity, students playfully simulate the process of dating samples "collected" from islands. They use measuring spoons (symbolizing the quantity of radiation damage per time) to fill clear plastic cups (i.e. the sediment sample) with beads (symbolizing radiation damage) to a pre-determined fill level. By counting the number of spoon-loads needed, students can determine the "age" of the sample. Ages are entered into a map and the results are discussed. Students determine from the results that an island is experiencing coastal erosion on its east side and depositing erosive outwash on the west side. This gives the impression that the island is "moving" west, and provides students insight on local geographic processes along the coast, and how geochronology helps measure and predict the outcome of such processes. I have tested the activity in a variety of settings and I have found the project to work well in general. This manuscript describes the different stages of the outreach event – i.e. introduction, hands-on activity and discussion – and the rationale behind each step, as well as the materials needed. Based on this description it is easily possible to adapt the activity for more advanced audiences or other geographic settings.

2. Materials needed

The materials needed fall under two main categories: (1) objects for the lesson introduction, to explain the basic principle of luminescence dating; and (2) materials for the hands-on activity. Materials in the first category can be found in most OSL labs, while materials for the second category were selected to be widely available and inexpensive.

Materials for Part 1 – explanation of radioactivity and luminescence dating:

- Geiger counter with the speaker tuned on

- materials with various levels of radioactivity that are also of general interest: e.g. uranium ore, Fiesta™ dinner ware, watches with a radium dial, a mammoth bone, piece of granite, sand samples, etc.

- fluorescent minerals and a UV flashlight (e.g. calcite, fluorite, sodalite)

Materials for Part 2 – hands-on activity:

- clear plastic cups

- measuring spoons of different sizes

- plastic beads or wood beads

- sticky notes and pens

- one or two posters showing sites and locations for collected samples

3. Part 1: Explanation of radioactivity and luminescence dating ($\sim$15 min)

The introduction includes multiple demonstrations and should not exceed 15 min, in order to leave enough time for the activity. The purpose of this part is for the students to understand why we need geochronology, and they should gain a very simple understanding of OSL dating. To establish continuous interaction with the students, I ask leading questions and give students the chance to contribute. In the hands-on part of the activity, which is explained in Section 4 in more detail, students use plastic cups, beads and measuring spoons to simulate the process of dating a sample. While I explain the basic principles, I frequently refer to the materials they will use later in their activity, and I demonstrate how they relate to the dating process. This process is illustrated in Figure 1.

The explanation of the basic principles is broken down into three steps which are outlined in the following:

1. **Explain the need for sediment and rock dating:** Purpose of the first step is to connect our activity to the real world and explain why we are doing luminescence dating. I choose regionally relevant examples for landscape change. Examples include the flooding events of September 2024 in Western North Carolina, or hurricanes and the resulting destruction of structures and roads. In a discussion we establish together that each event leaves behind a characteristic sediment layer. We can observe sequences of these sediment layers and see how often these events happen. To answer the question "how often", we need to know the age, and this is why we use methods such as luminescence dating.

2. **Introduction to radiation:** Children of the target age range have generally heard about radiation and radioactivity and the associated dangers. Using the Geiger counter and different materials, I demonstrate how radioactivity can range from high to low (this aspect is further discussed in Section 5). To explain the concept of dose rate, I take one of the clear cups, which represents a sample. Every time the counter clicks, radiation damage is done to the sample, and this is represented by the beads. For every click I throw a bead into the cup. If there is a lot of radioactivity more beads are thrown in. We discuss that, how quickly a cup fills, depends on the radioactivity of the sample. And the longer a sample is exposed to radioactivity, the more damage is accumulated. Thus, amount of damage can be used to measure time.

3. **Simplified introduction to luminescence:** Having established that damage can be used to measure time, we need to find a way to measure the damage. Children of the target age range have generally no knowledge
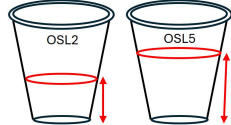
OSL dating	Sample collection	D_e How much radiation damage is present?	Dose rate How much damage is caused in a certain amount of time?
Activity	Map with "sampling sites" highlighted as X / Each cup represents one sample	Cups are marked with different fill levels prior to handing out to students	Scoops of different sizes indicate how much damage is done per unit time

Figure 1: Various steps of the OSL dating process and illustration how the materials used in the hands-on activity relate to each step.

of atomic structure or crystal structure. It was therefore necessary to simplify the explanation of the luminescence process. Fluorescent minerals are used to demonstrate the basic idea behind the OSL measurement: we stimulate with light of one "color" (UV flashlight), which causes the damage to heal; we obtain light of a different "color" (here fluorescence, which symbolizes the emitted luminescence). The more damage the sample had accumulated, i.e. the fuller the cup is, the brighter it glows. This is also a good moment to explain the need for collecting the samples in the dark and for working in a dark laboratory.

At the conclusion of part 1, the students should understand that we need two pieces of information in order to obtain an age: (1) How much radiation damage did the sample experience? / How full is the cup? (2) How much damage is done by radiation every year? / How big is the spoon that fills the cup?

4. Part 2: Hands-on activity (30–45 min)

In this part of the lesson, the students take on the role of the scientists. They are given a scientific question that requires geochronometry and they apply the principles learned in the introduction. They will first "date" samples and subsequently interpret the results to answer the question. So as not to exceed the 1-hour time limit, part 2 is designed to take 30–45 min.

4.1. Presenting the scientific question (∼5 min)

Due to our location on the East Coast of the USA and our closeness to the ocean, I developed an activity that centers on the guiding question "Do islands move?". The message of the question is easy to grasp for younger audiences - children will of course think that islands do not move.

My selection of the scientific question was informed by my aim to build on prior knowledge of the children. The

Outer Banks are barrier islands along the NC Atlantic Coast. They are familiar to students in Eastern North Carolina, as they are popular vacation and weekend spots, and most of the children have been there. The islands have become famous through movies, such as *Nights in Rodanthe*, and have drawn attention due to major damage caused by the last hurricanes. The children are generally aware of these facts. They do not usually know, however, that the islands formed at the end of the last ice age and experience a complicated pattern of overwash and long-shore transport (Riggs et al., 2011). Overwash acts like a conveyor belt and slowly moves the islands to the west, towards the mainland. These islands move!

At the beginning of the hands-on activity, the students are shown the two maps in Figure 2. They are told that one island (Island 1, Fig. 2 left) is a typical island that could be found somewhere in the ocean. Island 2 (Fig. 2 right) mimics an island on the Outer Banks of the North Carolina coast. I explain that I have already collected sediment samples from these locations and the sites are indicated on the maps with an X and a number. Their job is to "date" the samples and to enter the ages on the maps.

4.2. Dating the samples (15–20 min)

The materials for the dating activity are shown in Figure 3 and an outline of the process is given in Figure 4. I explain that the measurement of the radiation damage, i.e. the fill levels of the cups, has to be performed in the dark and requires specialized instrumentation. Therefore, I have already performed this task for every sample and every cup is already marked with sample number and a fill level. The spoons show us, how much damage is done in a certain amount of time. Each sample has a different spoon and the sample numbers on cups and spoons must match. The task is to find out, how many spoon loads are required to reach the respective fill level. From the label on the spoon, the age can be calculated as demonstrated in Figure 4. The sample number and age are then written on a sticky note and added to the correct spot on the map.
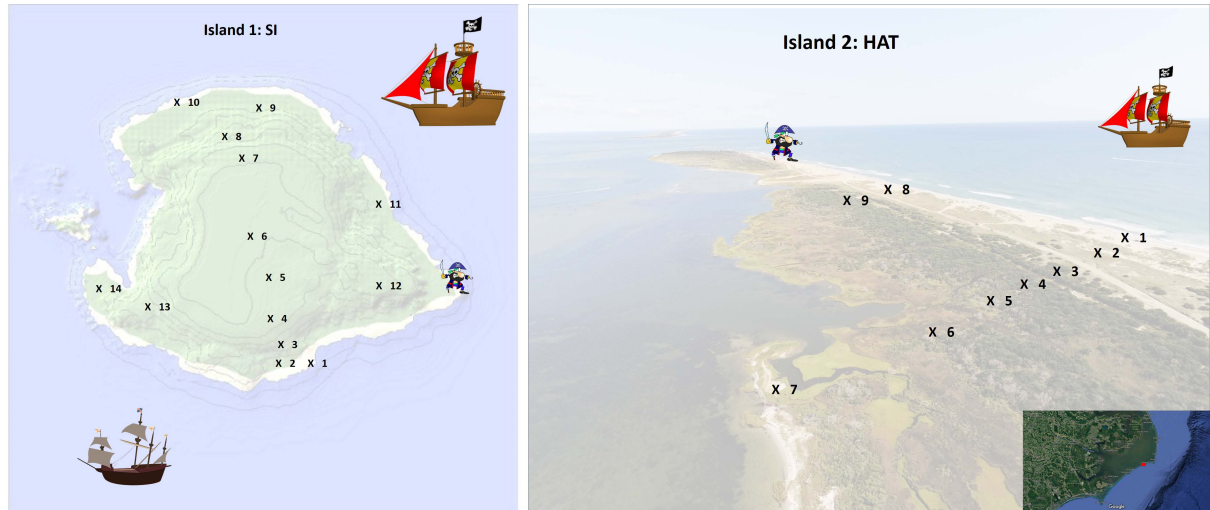
Figure 2: The two locations from which samples have been "collected" and which need to be "dated" by the students. Island 1 on the left represents a generic island that does not display major change over time ("SI" – Static Island). Island 2 on the right ("HAT" – Hatteras Island) is representative for the Outer Banks along the coast of North Carolina. These islands show dynamic behavior. They move! Sample locations are indicated with X and a sample number.

First, we work on one example together, to ensure that all students understand the task. The students are then divided into groups. Group sizes can range from two students up to six students, depending on the total number of children present. Each group is given a set of samples, which can vary from two to five samples, and the students have 15–20 min to complete their task.

4.3. Data analysis and discussion (10–15 min)

Once all ages have been entered into the map, the results are discussed, and the class answers the question "Do islands move?".

Island 1 is intended to be a generic non-changing island. Ages in years are shown in Figure 5. The discussion first focusses on the modern samples with age 1 year. These modern ages are used to re-affirm the concept that age refers to the time since the last light exposure. We discuss, why samples at the beach are so young. Next, we focus on the ages in the center, 250,000–300,000 years. These show that the largest part of the island is old and has not changed. Lastly, we discuss the intermediate ages (200, 500 and 5000 years). We discuss storm events and tsunamis that do not reach the higher parts of the island.

Island 2 represents the dynamic Outer Banks (Fig. 6A). A modern sample is located directly at the beach. All other samples show that the island is older on the eastern side, i.e., the ocean side, and younger towards the west, i.e., landwards. I let the children come up with ideas, how such an age sequence could happen. Some groups make creative suggestions (e.g., tsunamis), and we discuss if those could be possible. In general, the groups need to be guided towards the answer with leading questions. At the end I explain how wind and waves transport sand across the island, eroding the east

side and depositing on the west side, similar to a conveyor belt (Fig. 6B). This island moves!

5. Discussion

5.1. Did I meet my original aims and objectives?

The basic requirements and aims for my activity were: (i) The activity must be appropriate for 4th–8th graders and build on their prior knowledge; (ii) it must accommodate groups of up to 50 children; (iii) the whole event should take less than an hour; (iv) there must be "aha-moments" for the students to make a meaningful connection of the new concepts to the world around them. After the activity the children should have a basic understanding of the purpose of geochronology, of how results are interpreted, and of luminescence dating as an example of a geochronological method.

I have tested the activity with more than ten school classes, ranging in age from 4th to 8th grade, with groups ranging from 15 to 50 students, in my lab and in school classrooms. I did not attempt to formally assess the efficacy of the activity. However, I have been able to obtain feedback from the students and the teachers through conversations and unsolicited e-mails, which are discussed in more detail in the next paragraph. While minor tweaks are necessary to accommodate each individual setting, I have found the project to work well in general.

The time frame of below one hour ensures that students do not lose interest. While it is possible to reduce the time to 45 min, it seemed rushed, and I had to urge the children to complete the hands-on activity as fast as possible. During the activity students are divided into groups. To address varying class sizes, I have maps with different numbers of samples and I also have to adjust the number of samples per
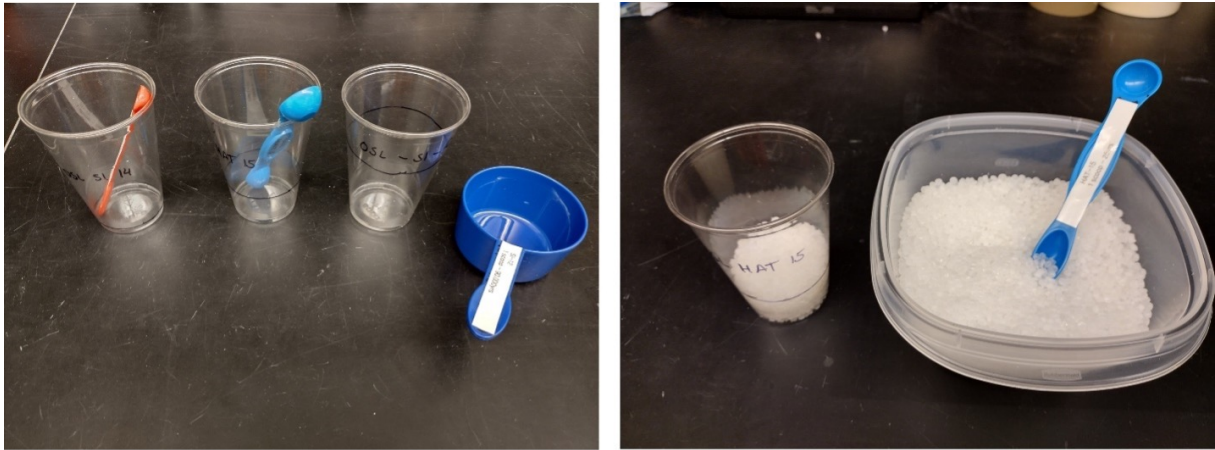
Figure 3: Sample cups and associated measuring spoons. Each sample comes with a dedicated spoon. Children use the spoon to fill the cup to the marked level with plastic beads. The label for sample spoon HAT 15 reads "1 scoop = 25 years".
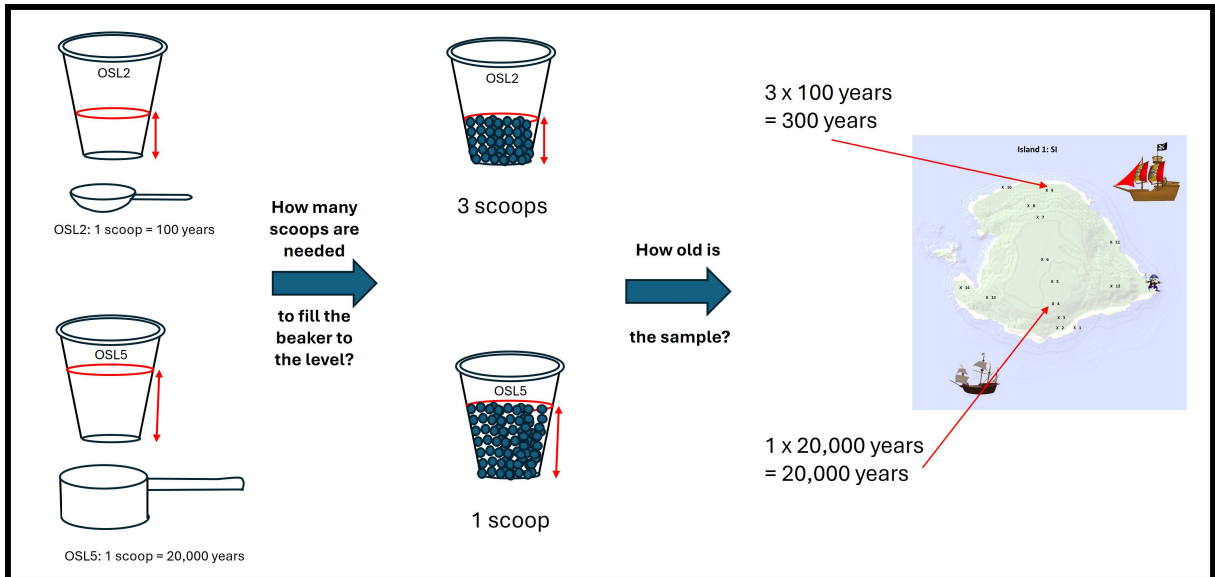
Figure 4: The steps taken to "date" a sample. Students count the number of spoons required to fill the cup to the indicated level. From the number of spoon loads and the label on the spoon the age is calculated and entered on the map.

group, which can range from two to five samples. Students generally like to see a real Geiger counter and unusual radioactive materials such as Fiesta[TM] dinner plates. They like looking at fluorescent minerals and if time allows at the end, they get the opportunity to try the UV flashlights themselves. Students particularly like the hands-on aspect of the event. While the plastic beads can be quite messy (having a broom at hand is imperative), students also consider them the most fun part of the activity.

The first step in developing the activity was the selection of the scientific question. As mentioned earlier, I wanted the children to be able to relate to the geographic location for a real-world connection. But I also wanted to introduce an aha-effect. The fact that almost all the kids are familiar with the Outer Banks, but likely do not know that these islands

move, fulfilled both requirements. This part of the activity is the only part that would have to be changed, when adopted by other laboratories. I did not aim at getting the ages and the geologic setting perfectly correct. On the contrary, I tried to simplify the age chart as much as possible. The static island is completely generic. Students of the target-range cannot yet visualize the difference between 100 million years and 100,000 years (e.g., Trend, 1998; Dodick and Orion, 2003). Both represent a large number, which translates into "old," which was completely sufficient for my purpose. For Island 2, the island representing the Outer Banks, I tried to stay within the approximately correct age range, but I did not perform a detailed literature search or use actual published ages. My main goal was to demonstrate an age gradient from east to west. I ignored long-shore transport, effects of inlets, etc.

Figure 5: Results for Island 1. The numbers indicate ages in years.

For older audiences more detailed maps with actual research results could be used and more detailed geologic processes could be discussed. Some gr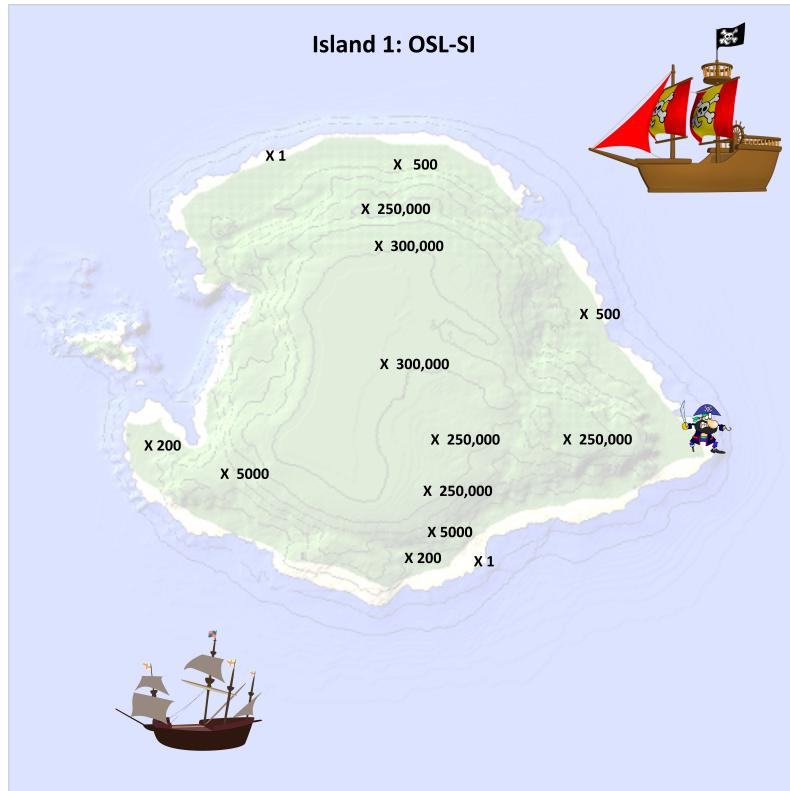oups needed nudging to understand that this island moves, others – including 4th graders – were able to draw this conclusion by themselves. But all classes were surprised by the fact that islands can and do move and that there are even such islands near-by!

5.2. Considerations for the hands-on activity

I always ask ahead of time how many students and teachers will participate. I determine how many groups should be formed and I pre-arrange "kits" with cups, spoons and beads. Part 1 involves all students at the same time. If necessary, for example in a larger room, I stand on a table or chair, to ensure that all children can see the demonstrations. The same is true for the discussion at the end. For the hands-on activity, the children are divided into smaller groups. For this purpose, I rely on the help of teachers, who have proven very effective in forming groups and making sure that the children follow the instructions. The transition from Part 1 to the hands-on activity usually takes no more than a few minutes. The boxes with the materials are handed out at the beginning of the hands-on part. Distributing the materials before the children arrive was not a good idea. The children did not pay attention to the explanation in Part 1 and played with the plastic beads instead. The activity requires little space. As long as enough separate tables are available, each individual group can easily work around a single table. Alternatively, students can sit on the floor. The teachers generally work together with the children. At the end, the children are asked to put all materials back in the boxes. I modified the activity several times to address reactions of students and to ensure that they really understood how the hands-on part relates to luminescence dating.

Most students were excited to see a real Geiger counter in use, in particular the feature of the loudspeaker that allows them to "hear" the radioactivity. They were fascinated by the low click-rate for sediment samples and the much higher click-rate for the mammoth bone. Quite a few students became apprehensive about the high count-rates for a piece of uranium ore. At this point I try to add small pieces of historic information about the years after the discovery of radioactivity. I mention the fact that radioactive toothpaste was sold, because it made the teeth glow at night, and I demonstrate the radioactivity of the Fiesta$^{\text{TM}}$ dinner plates. I tell them that for a while it was not uncommon to X-ray children's feet upon buying new shoes. And I explain about the women who painted radium-dials on clocks. All this highlights that we are now much more aware of the risks of radioactivity, and it serves to re-assure the students that I would not expose them to dangerous levels of radiation.

I tried illustrating the principle of luminescence by using dosimeters with a bright TL signal that is visible with the naked eye, such as TL from doped $CaSO_4$. I irradiated the dosimeters to saturation and used a laboratory heating
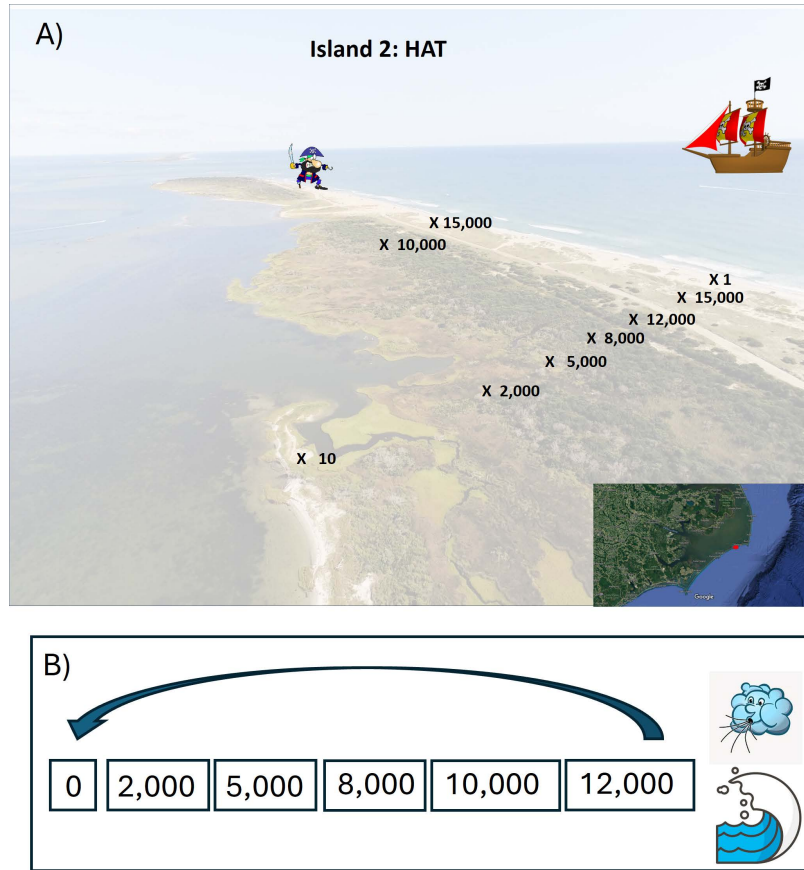
Figure 6: A) Results for Island 2. The numbers indicate ages in years. B) Illustration of the conveyor belt model to explain the age sequence.

plate. Unfortunately, even these very bright dosimeters appear very dim to the eye. The demonstration required a completely dark room, which is rarely available. Students did not have the patience to allow their eyes to become sufficiently adapted to the dark, I had to prevent them from touching the heating plate or pulling out their cell-phones. Many students were not able to see the dim TL emission. For these reasons I decided that UV-induced fluorescence is a more suitable proxy. I am using common and bright fluorescent minerals such as calcite and fluorite. It is not necessary to make the room completely dark, but it is advisable to close blinds or, at a minimum, to turn off lights, so that all children can see the glow. One of my samples is brighter, which I use to highlight that this reflects more radiation damage. For the activity the children only need to understand that radiation damage correlates with age. To avoid confusion, I keep the explanation of the luminescence process as simple as possible. For example, I do not mention that different minerals have different intrinsic brightness.

The materials for the dating activity are inexpensive and easy to find. Plastic beads can be replaced with more environmentally friendly materials such as wood beads. I originally used small pebbles to represent radiation damage, but students were confused about the difference between the ac-

tual sediment samples that we collect for OSL dating, and the pebbles that were meant to merely represent radiation damage. I decided to use an artificial material to avoid confusion. It is imperative to keep cup-and-spoon pairs together and to emphasize that the students need to match the sample numbers before starting the "dating process". Labelling the cups and spoons was somewhat time-consuming. I first had to decide on an age for that specific sample, then the cup had to be filled with an easy to measure number of spoon-loads, the level was marked, and last I had to convert age and number of loads to a "dose rate" for the spoon label. I chose simple numbers for both, number of spoon loads and the dose-rate, to ensure that the calculation did not pose a challenge for 4th graders. Marker labels on the spoons smudged after the first use and I decided to re-label them with printed labels. This might also be advisable for the labels on the cups, although the marker has held up well on the cups.

Instead of using printed maps and sticky notes, Powerpoint maps could be projected, and ages could be entered directly on the map. This depends on the facilities provided. When visiting schools, I found myself in a gym without the option to use a computer or projector. I also found that sticky notes give the students the feeling, that they actually contributed to this work and that they are looking at their own

data. They were more engaged than when projectors were used. Overall, it is helpful to know ahead of time, how many students will participate and what facilities are available if the event is held off-campus. It is also advisable to warn the teachers ahead of time about the radioactive materials and the Geiger counter to ensure that these items are not in conflict with school regulations.

6. Conclusions

I developed a simple hands-on activity for 4th–8th grade children with the goal to teach them about the need for geochronology and the basic principles of OSL dating. The children are first introduced to basic concepts and participate afterwards in a "dating" activity to answer a scientific question. In the hands-on part of the activity, students use measuring spoons to fill clear plastic cups with beads to a pre-determined fill level. By counting the number of spoon-loads needed, students can determine the "age" of the sample. Ages are entered into a map and the results are discussed. The scientific question, in our case "Do islands move?", was selected to be regionally relevant while also providing a moment of surprise that would re-inforce the lesson. The whole activity lasts approximately one hour and can accommodate groups with as many as 50 students. While minor tweaks are necessary for each individual case, I have found the project to be versatile and suitable for a variety of school settings. The activity can easily be adopted by other researchers. I recommend however that the scientific question be modified to fit the regional setting of each laboratory.

References

Dodick, J., Orion, N., 2003. Measuring student understanding of geological time. Science Education 87, 708–731. doi: https://doi.org/10.1002/sce.1057.

Edwards, S., 2015. Active learning in the middle grades. Middle School Journal 46, 26–32. doi: 10.1080/00940771.2015.11461922.

Pilcher, J., 2015. A Modified Delphi Study to Define "Ah Ha" Moments in Education Settings. Educational Research Quarterly 38, 51–67.

Riggs, S.R., von der Porten Ames, D., Culver, S.J., Mallinson, D.J., 2011. The battle for North Carolina's Coast: Evolutionary history, present crisis, and vision for the future. UNC Press Books.

Trend, R., 1998. An investigation into understanding of geological time among 10- and 11-year-old children. International Journal of Science Education 20, 973–988. doi: https://doi.org/10.1080/0950069980200805.

Ancient TL

Spotlight Review

Not fade away – The persistence of fading in feldspar luminescence

Svenja Riedesel[1,2]*

[1]Luminescence Physics and Technologies, Department of Physics, Technical University of Denmark, Lyngby/Roskilde, Denmark
[2]Institute of Geography, University of Cologne, Cologne, Germany

*Corresponding author: svenja.riedesel@uni-koeln.de

Abstract

Feldspars are widely used as natural luminescence dosimeters to constrain past geological, geomorphological and archaeological events and processes. Unfortunately, the luminescence of feldspars suffers from an unwanted signal loss over time, termed fading, which affects the reliability, precision, and accuracy of all these applications. This review presents an overview of the research conducted into the cause of and the physical processes behind fading, as well as of research focussed on circumventing, minimising or correction for fading. Fading has been shown to be ubiquitous in feldspars, affecting both thermoluminescence as well as optically (infrared) stimulated luminescence signals. The most widely accepted physical explanation for fading is quantum mechanical tunnelling of trapped electrons from the ground state of the electron trapping centre to a nearby recombination centre, however, other mechanisms have been proposed, and some of these different explanations are outlined here. Since fading causes an underestimation of the luminescence age, it is necessary to accurately constrain the rate of fading for a given sample, as well as to develop robust methods for correcting the obtained luminescence signal for fading. This review explains how the rate of fading can be determined in the laboratory, and how this can be used to correct the obtained luminescence signal or luminescence age for fading. This review aims at presenting key findings and selected studies as a means to introduce the topic to new researchers in the field of luminescence dating, while hoping that more experienced luminescence researchers might also discover some new information.

Keywords: Feldspar, Luminescence, Fading, Fading correction, Dating, Chronometry, Geochronology

1. Introduction

Feldspars, the most abundant mineral group in the Earth's crust, are widely used in luminescence-based geochronological studies to constrain past geological, geomorphological or archaeological events and processes. Their ubiquity, the mostly bright luminescence signal, and a signal saturation at a few hundred Gy make them an often favoured target for dating purposes. However, an undesired signal loss over time complicates their applicability. For accurate luminescence dating, it is usually expected that charge trapped within defects in the crystal lattice is stable over geological time scales (i.e., hundreds of thousands of years), with Aitken (1985) suggesting that the lifetime of trapped charge should at least be one magnitude longer than the period to be dated. However, the luminescence signal of feldspars exhibits an unwanted signal loss over time, which is referred to as *(anomalous) fading*. Measurements of fading rates all over the globe have shown the ubiquitous nature of this process (e.g. Spooner, 1994; Huntley and Lamothe, 2001; Valla et al., 2016), questioning the validity of the term "anomalous" fading.

Fading, a known process in many luminescence phosphors (e.g., Riehl, 1970; Delbecq et al., 1974, for ZnS or KCl:AgCl and KCl:TiCl, respectively), has already been shown in the 1970s to affect the luminescence of feldspars

(e.g. Garlick and Robinson, 1972; Wintle, 1973). However, despite its ubiquity and the multi-decade long awareness of this process affecting the luminescence of feldspars, many aspects of it remain under debate.

This review aims to present (i) a historical overview of the observation of fading in the luminescence of feldspars, (ii) different physical explanations and models developed to explain the processes behind fading in feldspars, and (iii) methods developed to minimise or circumvent fading, or to correct for its effects on the luminescence signals or ages calculated.

2. First approaches to understand fading in feldspars

The first experimental observations of fading of the feldspar luminescence signal were published in the 1970s for both lunar and Earth feldspars. Garlick and Robinson (1972) showed that when TL curves are measured following storage at different isothermal temperatures the luminescence intensity decreases with increasing storage times, even for storage at ambient temperatures. Based on this experimental evidence, Garlick and Robinson (1972) proposed that two processes lead to the loss of trapped charge in these feldspars: a thermally activated process and a non-thermal process. The rate of decrease in TL intensity with storage time follows a power-law decay, thus decreasing linearly with log(time) (Garlick and Robinson, 1972), an observation which was further explored by Huntley (2006). Garlick and Robinson (1972) proposed a simple model explaining the athermal loss. They based their model on first order kinetics, with the electron-hole recombination occurring via ground state to ground state transition and the power-law decay being explained through the random spatial distribution of electron and hole trapping centres.

Wintle (1973) presented results of anomalous fading of the TL signal of various feldspars and other minerals. The 20 feldspar samples studied showed a loss of TL signal after four weeks of storage of < 5 % to 40 %. Interestingly, storing a sample of fluorapatite at 77 K, 173 K, and 255 K revealed a smaller loss of TL at lower temperatures, suggesting that the process is not strictly athermal. However, it is unclear if this is also the case for feldspars.

Later, Wintle (1977) expanded her research into fading in feldspars and performed TL measurements after storage at temperatures as low as 20 K and observed a loss of TL even at cryogenic temperatures, with the amount of lost TL being independent of temperature up to 255 K. Recording any phosphorescence which might be emitted by the samples during storage revealed that the phosphorescence accounts only for 5 % of the total TL signal measured for a given sample. Wintle (1977) thus suggested that fading is likely only a weakly radiative or even non-radiative process. She proposed three different possible explanations for the physical processes behind fading: i) diffusion of defects, ii) direct transfer of an electron from the ground state of an electron trap to a nearby recombination centre (as suggested by Garlick and Robinson, 1972), and iii) reduction of the number of available recombination centres (hole movement).

Visocekas (1985) further explored whether athermal tunnelling recombination causes "anomalous" fading and if yes, why the afterglow intensity observed by Wintle (1977) was too low to account for the observed fading. Visocekas (1985) introduced a model of radiative tunnelling-based electron-hole recombination. Furthermore, measurements of a potential tunnelling afterglow revealed that such a signal could not have been detected previously, because of a spectral shift in the emission. Whilst below ambient temperatures the luminescence is primarily emitted in the red and infrared part of the spectrum, temperatures above room temperature show larger visible and UV components, which are detectable using standard photomultiplier tubes. This is in line with an earlier suggestion by Riehl (1970), based on ZnS, that the tunnelling afterglow should occur at wavelengths longer than the measured thermoluminescence.

With these studies published in the 1970s and 1980s, the existence of fading of feldspar luminescence was proven and first explanations were given. The following decades, until today, have been characterised by studies working towards a better understanding of the physical processes that govern fading in feldspars and by research towards correcting for fading or isolating a non-fading feldspar luminescence signal.

Figure 1 shows a timeline from the 1960s until the 2020s, highlighting some of the published work on experimental observations of fading in feldspars, models proposed for explaining the mechanism behind fading, as well as studies exploring potential ways of minimising fading or correcting for it. The timeline also highlights some selected publications, which were instrumental in understanding luminescence processes (in feldspars).

3. Potential physical causes of fading

Fading is not only ubiquitous in feldspars, but also in other materials. Prior (and in parallel) to its observation in feldspars, fading has been observed in ZnS (Riehl, 1970), KCl:AgCl and KCl:TiCl (e.g., Delbecq et al., 1974), zircon (e.g., Templer, 1986), calcite (e.g., Visocekas et al., 1976; Visocekas, 1979), $CaSO_4$:Dy (e.g., Visocekas et al., 1983), α-Al_2O_3 (e.g., Wood et al., 1990), and many more. Based on experimental observations on these various materials, potential physical explanations behind the fading process and corresponding models have been developed.

3.1. Quantum mechanical tunnelling from the ground state and tunnelling afterglow

The most widely accepted explanation for fading in feldspars is quantum mechanical tunnelling. It describes the recombination of electrons and holes through the overlap of their wavefunctions. This process has been found to be accompanied by the emission of photons, referred to as
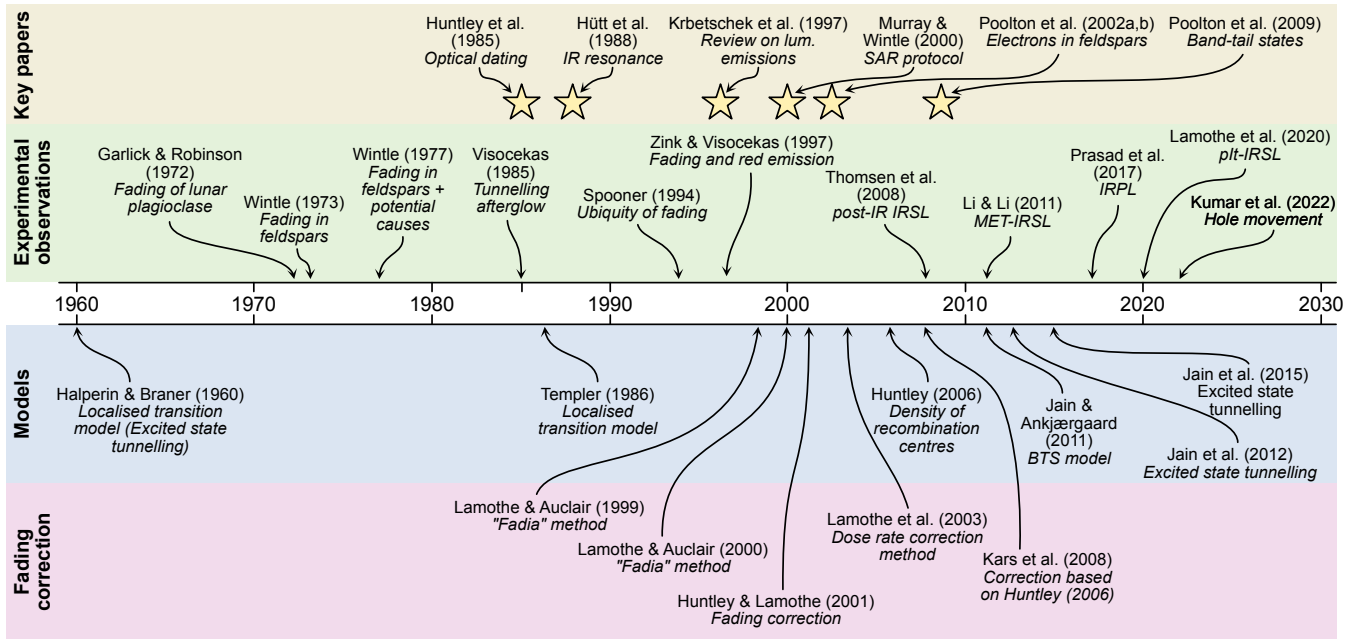
Figure 1: A timeline illustrating published research on experimental observations of fading in feldspars, the proposed models to explain the fading mechanism, and studies investigating potential methods to reduce or correct for it. Additionally, the timeline highlights key publications that have significantly contributed to understanding luminescence processes (in feldspars). Some terms have been abbreviated for the figure: IRSL = infrared stimulated luminescence, IRPL = infrared photoluminescence, BTS = band-tail states, MET = multiple elevated temperature, pIt-IRSL = post-isothermal IRSL.

tunnelling afterglow – the phosphorescence observed during storage at cryogenic temperatures (for example at liquid nitrogen temperature) following irradiation of the sample (e.g. Riehl (1970) for ZnS; Visocekas et al. (1985) for feldspars). Visocekas (1979) showed that the luminescence of calcite lost during storage is proportional to log(time). Following this, Visocekas (1985) suggested expressing fading as percent per decade of time, with the term decade describing the time steps from 1 to 10 to 100 etc. This power-law behaviour was used as argumentation for fading being caused by tunnelling of electrons from the ground state of the electron trapping centre to a nearby recombination centre (Fig. 2c), rather than by thermally induced detrapping. The latter would be expected to follow an exponential decay (see Aitken, 1985). The lifetime of the tunnelling process is thought to depend on the distance between the trapped electron and the trapped hole (Delbecq et al., 1974; Aitken, 1985).

Huntley (2006) proposed a theoretical model, which describes the power-law decay of luminescence and fading, based on tunnelling of electrons from the ground state of the electron trapping centres to nearby recombination centres (Fig. 2c). The model by Huntley (2006) is based on a couple of assumptions: (1) A crystal contains defects, which function as electron trapping centres, with electrons being trapped at some of these centres with an unknown distribution. (2) The crystal contains other defects, with a higher density and a random distribution to which electrons can tunnel. Since their density is assumed to be much higher than the density of trapped electrons, their density is assumed to be constant. (3) The tunnelling process is random with a lifetime, which is dependent on the attempt-to-escape frequency, the distance covered by the tunnelling process, and a constant which describes a sphere with a certain radius (referred to as α). (4) Electrons tunnel to the most proximal recombination centre. From these four assumptions, it is interesting to note that according to assumption (2) there would exist excess holes, causing charge imbalance of the crystal. Unless some of the defects acting as recombination centres would not contain a hole, but that would also make them unavailable for recombination, thus decreasing the density of centres available for recombination. For quartz it is suggested that so-called 'deep' electron traps exist, which are extremely thermally and optically stable (e.g., Bailey, 2001; Kijek and Chruścińska, 2017; Peng et al., 2022). Bailey (2001) reasons that during multiple burial-exposure cycles, the number of electrons trapped at these 'deep' traps increases, thus also increasing the number of trapped holes elsewhere in the crystal. It is unclear, if a similar system could exist in feldspars. Generally, the model by Huntley (2006) was developed to explain luminescence phenomena caused by ground state tunnelling, but it might be applicable to tunnelling of electrons from the excited state of the electron trapping centres to a nearby recombination centre (Fig. 2b), when the model is adjusted.
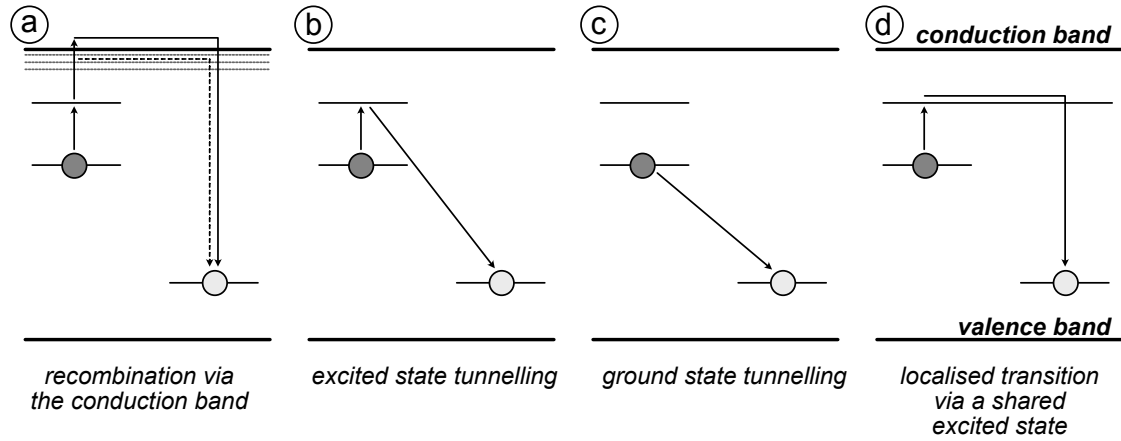
Figure 2: Schematic figure presenting the different luminescence processes considered for feldspars, specifically highlighting mechanisms proposed as explanation of fading in feldspars. (a) Recombination via the conduction band. Since this process is not occurring in feldspar IRSL, a recombination route via the sub-conduction band-tail states is indicated with dashed lines (cf. Jain and Ankjærgaard, 2011). (b) Tunnelling-recombination via the excited state (e.g., Halperin and Braner, 1960; Jain et al., 2012, 2015). (c) Ground state tunnelling (see Visocekas, 1985; Huntley, 2006). (d) Localised transition via an excited state common between the electron and the hole trap (following Templer, 1986).

3.2. Excited state tunnelling and other explanations

Halperin and Braner (1960) proposed a model which explains luminescence as the results of trapped electrons being thermally excited to the excited state of their trapping centre, from where they tunnel to a trapped hole, with this process being referred to as excited state tunnelling (Fig. 2b). Jain et al. (2012) used the model by Halperin and Braner (1960) as basis for their version of a localised transition model of feldspar luminescence. This model describes the luminescence resulting from excited state tunnelling taking place within randomly distributed donor-acceptor pairs, with the tunnelling distance dependent on the defect density, expressed as the density of recombination centres. The model was further extended by Jain et al. (2015) to account for truncated trapped electron-hole pair distributions, as these will be more likely, because fading (but also preheating in the laboratory) will have already caused the recombination of proximal electron-hole pairs. Other explanations for fading or models accounting for fading have been given. For example, Templer (1986) proposed a localised transition model, according to which trapped electrons can recombine with proximal holes via a shared excited state of the electron and hole trap (Fig. 2d). Kumar et al. (2022) investigated whether an unstable hole population is the cause behind fading in feldspars. They proposed that the blue luminescence recombination centre population is depleted due to fading between an electron trapping centre different to the one involved in infrared stimulated luminescence (IRSL) (and in infrared photoluminescence, IRPL), thus resulting in a reduced recombination efficiency for the trapped electrons and holes involved in IRSL. Already Wintle (1977) considered the possibility of fading being caused by the reduction of available hole centres.

3.3. Defect density, random distribution, and defect clustering

Most of the above presented models require a certain proximity between the electron trapping centres as donors and the recombination centres as acceptors. Two questions arise: (1) How close do these donor-acceptor pairs have to be to allow for tunnelling to occur, either from the ground or from the excited state? (2) How are these donor-acceptor pairs distributed within the crystal? For the latter question it should be mentioned that some of the earlier localised transition models assumed a fixed distance between donors and acceptors (e.g., Halperin and Braner, 1960), whilst others based their model on random distributions (e.g., Huntley, 2006; Jain et al., 2012).

Poolton et al. (2002) compared the possibility of both, ground and excited state tunnelling in feldspars, under the consideration of a simple electronic model assuming a defect analogous to a hydrogen atom. Using this, they calculated the extent of the electron wave functions of the ground and first excited state of such a defect, as the extent of these wave functions give information on the radius within which a recombination centre needs to occur to allow for the tunnelling process to take place (Fig. 3a). Poolton et al. (2002) thus presented the tunnelling recombination probability functions and inferred that the largest recombination probability from the ground state occurs at a distance of 1.6 Å, with only a 1 % probability of ground state tunnelling-based recombination to occur at a distance of 8 Å (Fig. 3a), with unit cell parameters for albite of $\sim$8.15 Å, $\sim$12.87 Å and $\sim$7.1 Å, for a, b, and c, respectively (Prewitt et al., 1976). For comparison, in microcline, these unit cell parameters are slightly larger with a, b and c being $\sim$8.57 Å, 12.97 Å, and 7.22 Å, respectively (Blasi et al., 1987). For the excited state, calculations by
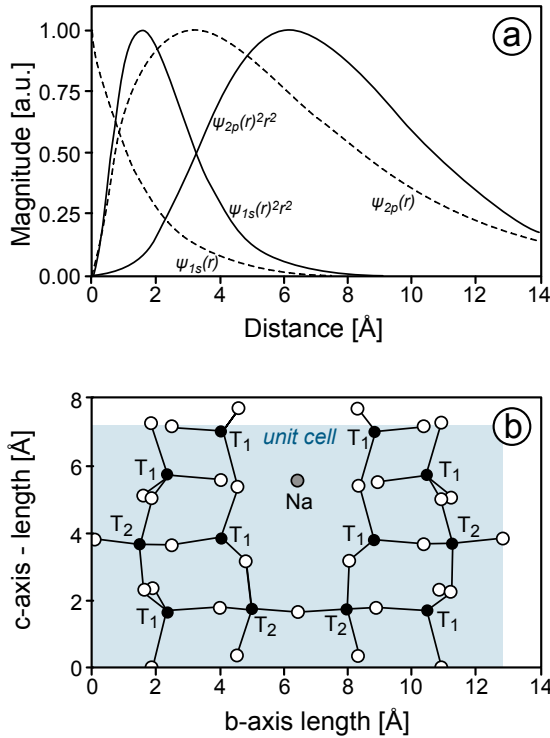
Figure 3: (a) Radial extent of the wavefunctions (Ψ) of the ground and first excited state of a trapped electron, calculated assuming a hydrogen-like model for Na-feldspar, by solving Schrödinger's equation. (b) Simplified crystal structure of Na-feldspar projected onto the (100) plane. Please note the same scale on the x-axis of both subfigures. The figures are redrawn from Poolton et al. (2002).

Poolton et al. (2002) predict the highest recombination probability to occur at a distance of 6.2 Å. According to these, there remains only a 0.03 % probability at 28 Å (Fig. 3a), which is just double the length of the longest unit cell parameter, *b*. Despite the simplicity of the hydrogen model, it becomes apparent that donor-acceptor pairs have to be within one unit cell (Fig. 3b), if recombination were to occur from the ground state of the electron trap, and within two unit cells, if the excited state would be considered.

These direct donor-acceptor recombination models require a high enough defect density to allow for this direct transition. Based on TL intensity, Sanderson (1988) calculated the number of electron and hole pairs (in his example: 10^7–10^8), which would participate in the luminescence process. For a sample which consist of $\sim 10^{20}$ atoms, this would result in a distance of 10^4 atoms when a random distribution of the electron hole pairs is assumed – a distance too large to be covered by direct donor-acceptor tunnelling recombination. If the ionisation density and the donor and acceptor defects are randomly distributed, then one would see a strong dependence of fading on the size of the dose given (Sanderson, pers. comm.). Alternatively, defects could occur clustered in certain regions of the crystal, resulting in

shorter electron-hole pair distances in such areas (see Sanderson, 1988).

Wintle (1977) tested potential dependences of fading on differently ionising irradiation types (α, β, γ) and found fading rates within 5 % of each other, suggesting no dependence of fading on the quality of irradiation. Visocekas (1988) showed that average fading rates of TL in CaSO$_4$:Dy doubled when irradiated using α-particles, compared to β-particles. Morthekai et al. (2013) performed fading tests for the IRSL signal of feldspars following irradiations with different ionisation densities (β-particles, X-rays and protons). They found that fading rates increased with increasing ionisation densities and concluded that fading does not occur across strongly coupled donor-acceptor pairs with constant donor-acceptor distances. The observed strong correlation between ionisation density (and thus trapped charge density) and fading rate is, according to Morthekai et al. (2013), an indication of a random distribution of defects. However, these observations only dismiss models assuming a fixed donor-acceptor distance (e.g., Randall and Wilkins, 1945; Halperin and Braner, 1960). They do not dismiss the idea of defect clustering in certain areas of the crystal (see Sanderson, 1988).

Besides the effect of different radiation types, studies have explored the effect of dose size administered with the same ionisation density (β-particles): Huntley (2006) observed an increase in IRSL fading rate with increasing dose for a feldspar sample. They further were able to show that the fading rate of a feldspar sample in field saturation (the equilibrium state between electron trap filling due to dosing and trapped charge depletion due to thermal annealing and fading) was higher when the sample had been bleached. Based on the models proposed by Huntley (2006) and Kars et al. (2008) and on own experimental data, Li and Li (2008) observed a dose-dependency of fading rates of natural and laboratory irradiated feldspars. They explained this increase in fading with increasing dose with the greater number of electron-hole pairs generated by large doses. They furthermore proposed that there exists a competition between stable and unstable electron traps in feldspars. At low doses and over short irradiation times, it will be similarly likely to have electrons trapped at both these types of traps. On the contrary, at high doses, charge trapped at stable electron traps will remain there whilst electrons will continue to fade out of the unstable traps, making electron trapping at these unstable traps more likely during longer irradiation times.

4. The *g*-value – Means to quantify the fading rate

Despite the ongoing debate of the physical processes governing fading in feldspars, the loss of luminescence signal at ambient temperatures affects the application of feldspars in luminescence dating. Thus, efforts have been made to quantify the signal loss and to correct for it. This chapter presents the method by Auclair et al. (2003), which is widely used for

estimating the rate of fading over laboratory time scales.

Usually, the fading rate is expressed as the *g*-value, which corresponds to the percentage of luminescence lost due to fading per decade of time (Aitken, 1985; Visocekas, 1985). The *g*-value can be obtained by fitting a series of L_x/T_x values, obtained after repeated regenerative doses of the same size, but after different delay (or storage) times between the irradiation and the luminescence measurement, and their respective storage times, using Eq. 1 (Auclair et al., 2003):

$$I = I_c \left[1 - \frac{g}{100} \log_{10} \left(\frac{t}{t_c} \right) \right] \quad (1)$$

In this equation, *I* represents the luminescence intensity measured after time *t*. I_c refers to the luminescence intensity when $t = t_c$. According to (Auclair et al., 2003), t_c is an arbitrary time, but usually the time since irradiation for the prompt measurement is used. However, this time may vary for different aliquots or samples measured, or dependent on the instrument used for the measurement or the size of the irradiation dose. Thus, it is suggested to normalise t_c to a fixed value, and here commonly a t_c-value of 2 days is used (Huntley and Lamothe, 2001; Auclair et al., 2003).

For constraining the *g*-value, it is crucial to properly estimate the time between the irradiation and the luminescence measurement, usually referred to as time since irradiation, and introduced as t^* (Aitken, 1985). There exist two possibilities of deriving t^*. Following Aitken (1985), and modified by Auclair et al. (2003):

$$t^* = t_0 \cdot 10 \left[\frac{t_2 \log \left(\frac{t_2}{t_0} \right) - t_1 \log \left(\frac{t_1}{t_0} \right) - 0.43(t_2 - t_1)}{t_2 - t_1} \right] \quad (2)$$

Here, $0.43 = \frac{1}{\ln(10)}$. Additionally, t_0 can be set to 1, as it is regarded as an arbitrary constant (cf. Auclair et al., 2003). Equation 2 can thus be shortened to:

$$t^* = 10 \left[\frac{t_2 \log t_2 - t_1 \log t_1}{t_2 - t_1} - \frac{1}{\ln 10} \right], \quad (3)$$

as given in the Analyst manual (Duller, 2016). The second possibility is an approximation presented by Auclair et al. (2003):

$$t^* \cong t_1 + \frac{t_2 - t_1}{2} \quad (4)$$

The parameter t^* can be estimated using either Eq. 3 or 4, with the parameters of these equations being displayed in Figure 4.

Auclair et al. (2003) furthermore explored different possible measurement designs for the determination of fading for a given sample. They observed that the *g*-value is dependent on the method used, with the most robust results being obtained using a SAR procedure (see Murray and Wintle, 2000; Wallinga et al., 2000) during which the sample is stored for different periods of time following irradiation and preheating.
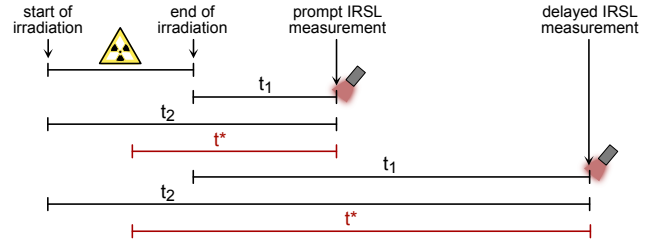
Figure 4: Graphical representation of the parameters involved in the calculation of t^*. The length of the timelines is arbitrary. The figure has been modified from Auclair et al. (2003).

5. Correcting for fading

Different methods for correcting the feldspar IRSL signals for fading were developed. This includes an isochron method termed "fadia" (Lamothe and Auclair, 1999, 2000), which was further investigated by Lamothe et al. (2012) and Li et al. (2016), as well as the dose rate method by Lamothe et al. (2003). However, for the purpose of this review, we will focus on the two most commonly used correction methods, which are also applicable to SAR-based IRSL results: The fading correction method by Huntley and Lamothe (2001) and the method by Huntley (2006), which was adapted for dating purposes by Kars et al. (2008).

5.1. Fading correction following Huntley and Lamothe (2001)

The fading correction method by Huntley and Lamothe (2001) is based on the quantum mechanical tunnelling model. It is predicted that the luminescence intensity *I*, measured over time *t* follows Eq. 5, where *k* is a constant, which is sample-dependent and varies with t_c. I_c is the intensity when time $t = t_c$.

$$I = I_c \left[1 - k \ln \left(\frac{t}{t_c} \right) \right] \quad (5)$$

For further details and a differential form of the equation, the reader is referred to the original publication by Huntley and Lamothe (2001). Regarding the correction of luminescence ages, Eq. 6 is used:

$$\frac{\text{measured age}}{\text{true age}} = 1 - k \left[\left(\frac{\text{true age}}{t_c} \right) - 1 \right] \quad (6)$$

Here "true" age denotes the luminescence age, if no fading had occurred. The parameter t_c is chosen as the time between the laboratory irradiation and the luminescence measurement, whereas *k* is defined dependent on t_c. In their example, Huntley and Lamothe (2001) used $t_c = 2$ days. Since their study in 2001, fading rates obtained in various studies have conventionally been normalised to 2 days.

The model by Huntley and Lamothe (2001) assumes that the fading rate is constant over the initial part of the dose re-

Figure 5: Following Huntley and Lamothe (2001), the decrease in luminescence (indicated as intensity) is predicted for up to 10^{13} da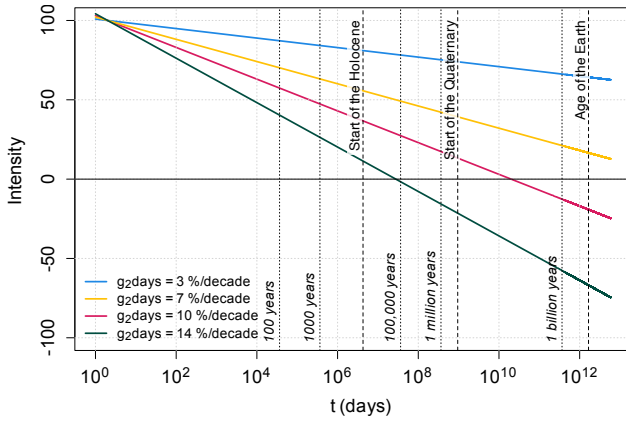ys ($\sim$27 billion years) for visualisation purposes using four different g-values. The g-values were normalised to 2 days and the t_c value was set to 2 days. For this prediction the following equation was used: $y = I_c \cdot (1 - (\frac{g}{100}) \cdot \log_{10}(\frac{t}{t_c}))$. Here, I_c was set to be 100. This figure shows that the model by Huntley and Lamothe (2001) results in large values at very short time scales (see mismatch between predicted lines) and negative values at very long time scales. The latter occurs only for very high g-values. In the case of smaller g-values, negative values will eventually be reached, but as the example shows, only at time scales irrelevant for luminescence dating.

sponse curve, which can still be fitted using a linear function. However, on short time scales their model predicts too large values (Fig. 5). Physically, this is explained by the probability of electron-hole pairs being very proximal (Huntley and Lamothe, 2001). At long time scales, their model predicts negative intensities (Fig. 5). At higher doses, trapped electrons have a chance of tunnelling to the nearby recombination centres, thus opening the possibility of their former trap to be repopulated and emptied by tunnelling again (referred to as repetitive filling and emptying by Huntley and Lamothe, 2001). Interestingly, Buylaert et al. (2008) have shown the successful applicability of this correction method to doses ranging from $\sim$100 Gy to $\sim$150 Gy.

5.2. Huntley (2006) and Kars et al. (2008) – Density of recombination centres

Huntley (2006) described electron-hole recombination due to ground state tunnelling in feldspars as a function of the lifetime of the tunnelling decay (τ), the distribution of distances (r) between electron and hole trapping centres, and the density of recombination centres (ρ'). According to Huntley (2006), fading and the number of electrons remaining trapped after time t depends on ρ'. Eq. 7 describes the relationship of the trapped electron density n remaining after time t, compared to the initial trapped electron population n_i. The parameter s represents the attempt-to-escape frequency,

which is assumed to be 3×10^{15} s^{-1} (Huntley, 2006).

$$\frac{n}{n_i} = \exp\left(-\rho' \left[\ln\left(1.8st\right)\right]^3\right) \qquad (7)$$

Equation 7 shows that n determined after delay time t is dependent on ρ', and the luminescence signal intensity (for example the IRSL intensity) is the result of the number of trapped charges recombining. Kars et al. (2008) rewrote Eq. 7 to:

$$\text{IRSL}_{\text{faded}} = \text{IRSL}_{\text{initial}} \cdot \exp\left(-\rho' \left[\ln\left(1.8st\right)\right]^3\right) \qquad (8)$$

$\text{IRSL}_{\text{initial}}$, the unfaded IRSL signal, is thus obtained by dividing the faded IRSL signal by $\exp\left(-\rho' \left[\ln\left(1.8st\right)\right]^3\right)$. This procedure can be applied to each point of a dose response curve. Correcting each point for the signal loss due to fading gives the unfaded dose response. The parameter ρ' is obtained by plotting L_x/T_x values measured during a SAR fading experiment against time and fitting the points using Eq. 8.

Furthermore, the model by Kars et al. (2008) allows for the construction of a natural dose response curve. For this approach the dose rate ($\dot{D}$) in Eq. 9 needs to be adapted to the natural conditions (see Kars et al., 2008; King et al., 2018). In Eq. 9, A is a pre-exponential factor, corresponding to the maximum asymptote of the dose response curve, and D_0 is the characteristic dose, which describes the curvature of the dose response curve.

$$\frac{L_x}{T_x}(t) = \exp\left(-\rho' \left[\ln\left(1.8st\right)\right]^3\right) \cdot A \left(1 - \exp\left(-\frac{\dot{D}t}{D_0}\right)\right) \qquad (9)$$

The model by Huntley (2006) and its adaptation for luminescence dating purposes by Kars et al. (2008) enable the fading correction of older samples. However, Li and Li (2008) raised criticism in response to the use of a constant ρ'-value for fading correction of older samples and for the construction of a natural dose response curve. They observed a dose dependency of fading rates, suggesting that ρ' will change over time during which a sample is exposed to ionising radiation (Li and Li, 2008). Thus, these authors suggested to determine ρ' for different regenerative doses – rendering the fading correction method more complex.

6. Methods for minimising or circumventing fading

Whilst fading correction is possible, it is advantageous if a non-fading luminescence signal could be used in dating applications. Despite the ubiquitous nature of fading, differences in fading rate between chemically and structurally different feldspars have been observed. Wintle (1973) reported high fading rates in feldspars of volcanic origin and Spooner (1992, 1994) observed differential fading rates between mineralogically different feldspars. These results are

supported by more recent work by Riedesel et al. (2021), who showed that IRSL fading rates depend on the structure of the feldspars investigated, with ordered K- and Na-feldspar end-members exhibiting only little to no fading. While this suggests that specific types of feldspars could be used for dating without having to correct for fading, the rarity of these feldspar types severely limits this approach. Other options, such as selecting grains based on their luminescence sensitivity (Lamothe et al., 2012) or detecting luminescence in specific emission windows (e.g., Spooner, 1992; Zink and Visocekas, 1997; Stokes and Fattahi, 2003) to minimise the influence of fading, have been suggested.

However, the focus has been on modifying measurement procedures for both TL and IRSL to circumvent or minimise fading, with most of them involving storage or preheat treatments to isolate a more stable signal (e.g., Clark and Templer, 1988; Molodkov and Bitinas, 2006). Further advances over the past two decades resulted in protocols using multiple successive IRSL measurements at increasing temperatures to separate a more stable feldspar IRSL signal for dating (Thomsen et al., 2008; Li and Li, 2011). The basis of these protocols, involving two consecutive (post-IR IRSL, Thomsen et al., 2008) or three to five consecutive IRSL measurement steps (multiple-elevated temperature, MET-protocols; Li and Li, 2011), is a random distribution of electron and hole traps in the crystal. The trapped electrons are understood to tunnel to the nearest recombination centre. The preheat and the following lower temperature IRSL measurement steps (e.g., 50 °C) will result in the recombination of trapped electrons with the most proximal holes (see Jain and Ankjærgaard, 2011), leaving only the more distal holes available for recombination during the higher temperature post-IR IRSL or MET steps. Since fading to these holes is less likely, due to the greater donor-acceptor distance, the thus obtained luminescence signal is expected to be more stable (cf. Jain and Ankjærgaard, 2011). These post-IR IRSL and MET-IRSL protocols have been widely applied, and lower fading rates were generally observed for the higher temperature IRSL steps (e.g., Buylaert et al., 2012). However, this is at the cost of signal bleachability, with higher temperature IRSL signals resetting slower during sunlight exposure, compared to signals measured at lower temperatures (e.g., Colarossi et al., 2015).

Interestingly, Lamothe et al. (2020) took advantage of the different fading rates of IRSL signals stimulated at different temperatures. They propose a measurement protocol, which facilitates a modified post-IR IRSL procedure to find a thermal treatment resulting in the same equivalent dose for the low and the high temperature IRSL measurements within a post-IR IRSL protocol: the post-isothermal IRSL (pIt-IRSL) protocol. Whilst the natural (L_n/T_n) cycle is measured following the conventional post-IR IRSL protocol, a thermal annealing step with different annealing durations at a temperature higher than the preheat is inserted after the L_x preheat. (Lamothe et al., 2020) tested the proposed protocol on three different samples and obtained ages in agreement with independent age control for two samples. The third sample

was used to test the validity of the protocol against signal saturation with satisfying results. Ataee et al. (2025) tested the pIt-IRSL on polymineral fine grain material and observed good performance of the protocol, as long as the first IRSL signal is not saturated. For this case, Ataee et al. (2025) presented a modified pIt-IRSL protocol.

All these methods use recombination-based luminescence, thus involving electron traps and hole traps in the luminescence production. To minimise fading, alternative, non-recombination based methods have also been explored. Infrared radioluminescence or radiofluorescence (IR-RF; Trautmann et al., 1998, 1999) measures the filling of a specific type of electron trap in feldspars. Here, luminescence is recorded in the infrared, which arises due to ionised electrons being trapped in electron traps below the conduction band. This type of electron trap can also be sensed using IRPL (Prasad et al., 2017; Kumar et al., 2018). IRPL arises from the non-destructive probing of the trapped electron population in feldspars by stimulating the sample with IR photons. For both methods only little information on fading is available. Krbetschek et al. (2000) reported that it was possible to date samples using IR-RF, which were expected to be saturated. Kumar et al. (2021) showed that IRPL measurements exhibit lower fading, compared to conventional recombination-based luminescence techniques. However, further studies testing the applicability of IRPL to date Pleistocene sediments need to be performed to fully evaluate its benefits.

7. Conclusions

This review presents an overview of the research history into fading of feldspar luminescence, as well as into the research developments of the past decades, which focussed on developing a better understanding of the physical processes behind fading in feldspars, the ubiquity of this phenomenon, and into ways of circumventing, minimising or correcting for fading. Particularly worth highlighting are the following points:

- Fading, a loss of the luminescence signal at ambient temperatures, does not only occur in feldspars, but also in other luminescence phosphors.

- Fading seems to be ubiquitous in feldspars, with very few examples showing low fading feldspars.

- Ground state tunnelling is the most widely accepted explanation for fading. However, it has been indicated that this process might have limitations, and that excited state tunnelling might be the more likely explanation.

- Fading appears to be dependent on the ionisation density and size of the irradiation dose administered.

- It is possible to constrain the rate of fading in the laboratory and to use this information to correct for fading that occurred over geological time scales.

- Different options are available to access a luminescence signal exhibiting lower fading rates, unfortunately, often at the cost of lower bleachability. However, it has not been possible to fully eliminate fading.

References

Aitken, M., 1985. Thermoluminescence Dating. Academic Press, London, United Kingdom. doi: 10.1016/C2009-0-06368-8.

Ataee, N., Roberts, H.M., Duller, G.A.T., 2025. Assessing the potential of a modified post-isothermal IRSL (pIt-IR) protocol to circumvent the problems posed by anomalous fading in polymineral fine grains. Quaternary Geochronology 88, 101676. doi: 10.1016/j.quageo.2025.101676.

Auclair, M., Lamothe, M., Huot, S., 2003. Measurement of anomalous fading for feldspar IRSL using SAR. Radiation Measurements 37, 487–492. doi: 10.1016/S1350-4487(03)00018-0.

Bailey, R.M., 2001. Towards a general kinetic model for optically and thermally stimulated luminescence in quartz. Radiation Measurements 33, 17–45. doi: 10.1016/S1350-4487(00)00100-1.

Blasi, A., De Pol Blasi, C., Zanazzi, P.F., 1987. A re-examination of the Pellotsalo microcline: Mineralogical implications and genetic considerations. The Canadian Mineralogist 25, 527–537.

Buylaert, J.P., Jain, M., Murray, A.S., Thomsen, K.J., Thiel, C., Sohbati, R., 2012. A robust feldspar luminescence dating method for Middle and Late Pleistocene sediments. Boreas 41, 435–451. doi: 10.1111/j.1502-3885.2012.00248.x.

Buylaert, J.P., Murray, A.S., Huot, S., 2008. Optical dating of an Eemian site in Northern Russia using K-feldspar. Radiation Measurements 43, 715–720. doi: 10.1016/j.radmeas.2008.01.027.

Clark, P.A., Templer, R.H., 1988. Dating thermoluminescence samples which exhibit anomalous fading. Nuclear Tracks and Radiation Measurements 14, 139–141. doi: 10.1016/1359-0189(88)90054-4.

Colarossi, D., Duller, G.A.T., Roberts, H.M., Tooth, S., Lyons, R., 2015. Comparison of paired quartz OSL and feldspar post-IR IRSL dose distributions in poorly bleached fluvial sediments from South Africa. Quaternary Geochronology 30, 233–238. doi: 10.1016/j.quageo.2015.02.015.

Delbecq, C.J., Toyozawa, Y., Yuster, P.H., 1974. Tunneling recombination of trapped electrons and holes in KCl:AgCl and KCl:TlCl. Physical Review B 9, 4497–4505. doi: 10.1103/PhysRevB.9.4497.

Duller, G.A.T., 2016. Analyst v4.31.9 user manual. Technical report. 83 pp.

Garlick, G.F.J., Robinson, I., 1972. The thermoluminescence of lunar samples. Proceedings of the International Astronomical Union 47, 324–329. doi: 10.1017/S0074180900097631.

Halperin, A., Braner, A.A., 1960. Evaluation of Thermal Activation Energies from Glow Curves. Physical Review 117, 408–415. doi: 10.1103/PhysRev.117.408.

Huntley, D.J., 2006. An explanation of the power-law decay of luminescence. Journal of Physics: Condensed Matter 18, 1359–1365. doi: 10.1088/0953-8984/18/4/020.

Huntley, D.J., Lamothe, M., 2001. Ubiquity of anomalous fading in K-feldspars and the measurement and correction for it in optical dating. Canadian Journal of Earth Science 38, 1093–1106. doi: 10.1139/cjes-38-7-1093.

Jain, M., Ankjærgaard, C., 2011. Towards a non-fading signal in feldspar: Insight into charge transport and tunnelling from time-resolved optically stimulated luminescence. Radiation Measurements 46, 292–309. doi: 10.1016/j.radmeas.2010.12.004.

Jain, M., Guralnik, B., Andersen, M.T., 2012. Stimulated luminescence emission from localized recombination in randomly distributed defects. Journal of Physics: Condensed Matter 24, 385402. doi: 10.1088/0953-8984/24/38/385402.

Jain, M., Sohbati, R., Guralnik, B., Murray, A.S., Kook, M., Lapp, T., Prasad, A.K., Thomsen, K.J., Buylaert, J.P., 2015. Kinetics of infrared stimulated luminescence from feldspars. Radiation Measurements 81, 242–250. doi: 10.1016/j.radmeas.2015.02.006.

Kars, R.H., Wallinga, J., Cohen, K.M., 2008. A new approach towards anomalous fading correction for feldspar IRSL dating – tests on samples in field saturation. Radiation Measurements 43, 786–790. doi: 10.1016/j.radmeas.2008.01.021.

Kijek, N., Chruścińska, A., 2017. On the equivalence of natural and laboratory growth curves in luminescence dating - The effect of deep traps and luminescence centres. Radiation Measurements 106, 477–482. doi: 10.1016/j.radmeas.2017.05.014.

King, G.E., Burow, C., Roberts, H.M., Pearce, N.J.G., 2018. Age determination using feldspar: Evaluating fading-correction model performance. Radiation Measurements 119, 58–73. doi: 10.1016/j.radmeas.2018.07.013.

Krbetschek, M.R., Trautmann, T., Dietrich, A., Stolz, W., 2000. Radioluminescence dating of sediment: methodological aspects. Radiation Measurements 32, 493–498. doi: 10.1016/S1350-4487(00)00122-0.

Kumar, R., Kook, M., Jain, M., 2021. Sediment dating using infrared photoluminescence. Quaternary Geochronology 62, 191147. doi: 10.1016/j.quageo.2020.101147.

Kumar, R., Kook, M., Jain, M., 2022. Does hole instability cause anomalous fading of luminescence in feldspar? Journal of Luminescence 252, 119403. doi: 10.1016/j.jlumin.2022.119403.

Kumar, R., Kook, M., Murray, A.S., Jain, M., 2018. Towards direct measurement of electrons in metastable states in K-feldspar: Do infrared-photoluminescence and radioluminescence probe the same trap? Radiation Measurements 120, 7–13. doi: 10.1016/j.radmeas.2018.06.018.

Lamothe, M., Auclair, M., 1999. A solution to anomalous fading and age shortfalls in optical dating of feldspar minerals. Earth and Planetary Science Letters 171, 319–323. doi: 10.1016/S0012-821X(99)00180-6.

Lamothe, M., Auclair, M., 2000. The fadia method: a new approach in luminescence dating using the analysis of single feldspar grains. Radiation Measurements 32, 433–438. doi: 10.1016/S1350-4487(00)00124-4.

Lamothe, M., Auclair, M., Hamzaoui, C., Huot, S., 2003. Towards a prediction of long-term anomalous fading of feldspar IRSL. Radiation Measurements 37, 493–498. doi: 10.1016/S1350-4487(03)00016-7.

Lamothe, M., Barré, M., Huot, S., Ouimet, S., 2012. Natural luminescence and anomalous fading in K-feldspar. Radiation Measurements 47, 682–687. doi: 10.1016/j.radmeas.2012.04.018.

Lamothe, M., Brisson, L.F., Hardy, F., 2020. Circumvention of anomalous fading in feldspar luminescence dating using Post-Isothermal IRSL. Quaternary Geochronology 57, 101062. doi: 10.1016/j.quageo.2020.101062.

Li, B., Li, S.H., 2008. Investigations of the dose-dependent anomalous fading rate of feldspar from sediments. Journal of Physics D: Applied Physics 41, 22502. doi: 10.1088/0022-3727/41/22/225502.

Li, B., Li, S.H., 2011. Luminescence dating of K-feldspar from sediments: A protocol without anomalous fading correction. Quaternary Geochronology 6, 468–479. doi: 10.1016/j.quageo.2011.05.001.

Li, B., Roberts, R.G., Brumm, A., Guo, Y.J., Hakim, B., Ramli, M., Aubert, M., Grün, R., Zhao, J.X., Saptomo, W., 2016. IRSL dating of fast-fading sanidine feldspars from Sulawesi, Indonesia. Ancient TL 34, 1–13. doi: 10.26034/la.atl.2016.503.

Molodkov, A., Bitinas, A., 2006. Sedimentary record and luminescence chronology of the Lateglacial and Holocene aeolian sediments in Lithuania. Boreas 35, 244–254. doi: 10.1111/j.1502-3885.2006.tb01154.x.

Morthekai, P., Jain, M., Dach, G., Elma, D.R., Prip, H., 2013. Dependence of (anomalous) fading of infra-red stimulated luminescence on trap occupancy in feldspars. Journal of Luminescence 143, 704–709. doi: 10.1016/j.jlumin.2013.05.040.

Murray, A.S., Wintle, A.G., 2000. Luminescence dating of quartz using an improved single-aliquot regenerative-dose protocol. Radiation Measurements 32, 57–73. doi: 10.1016/S1350-4487(99)00253-X.

Peng, J., Wang, X., Adamiec, G., Zhao, H., 2022. Critical role of the deep electron trap in explaining the inconsistency of sensitivity-corrected natural and regenerative growth curves of quartz OSL at high irradiation doses. Radiation Measurements 159, 106874. doi: 10.1016/j.radmeas.2022.106874.

Poolton, N.R.J., Wallinga, J., Murray, A.S., Bulur, E., Bøtter-Jensen, L., 2002. Electrons in feldspar I: on the wavefunction of electrons trapped at simple lattice defects. Physics and Chemistry of Minerals 29, 210–216. doi: 10.1007/s00269-001-0217-3.

Prasad, A.K., Poolton, N.R.J., Kook, M., Jain, M., 2017. Optical dating in a new light: A direct, non-destructive probe of trapped electrons. Scientific Reports 7, 12097 doi=10.1038/s41598–017–10174–8.

Prewitt, C.T., Sueno, S., Papike, J.J., 1976. The crystal structures of high albite and monalbite at high temperatures. American Mineralogist 61, 1213–1225.

Randall, J.T., Wilkins, M.H.F., 1945. Phosphorescence and electron traps I. The study of trap distributions. Proceedings of the Royal Society A 184, 366–389. doi: 10.1098/rspa.1945.0024.

Riedesel, S., Bell, A.M.T., Duller, G.A.T., Finch, A.A., Jain, M., King, G.E., Pearce, N.J., Roberts, H.M., 2021. Exploring sources of variation in thermoluminescence emissions and anomalous fading in alkali feldspars. Radiation Measurements 141, 106541. doi: 10.1016/j.radmeas.2021.106541.

Riehl, N., 1970. Tunnel luminescence and infrared stimulation. Journal of Luminescence 1, 1–16. doi: 10.1016/0022-2313(70)90019-0.

Sanderson, D.C.W., 1988. Fading of thermoluminescence in feldspars: Characteristics and corrections. Nuclear Tracks and Radiation Measurements 14, 155–161. doi: 10.1016/1359-0189(88)90057-X.

Spooner, N.A., 1992. Optical dating: Preliminary results on the anomalous fading of luminescence from feldspars. Quaternary Science Reviews 11, 139–145. doi: 10.1016/1350-4487(94)90111-2.

Spooner, N.A., 1994. The anomalous fading of infrared-stimulated luminescence from feldspars. Radiation Measurements 23, 625–632.

Stokes, S., Fattahi, M., 2003. Red emission luminescence from quartz and feldspar for dating applications: an overview. Radiation Measurements 37, 383–395. doi: 10.1016/S1350-4487(03)00060-X.

Templer, R.H., 1986. The localised transition model of anomalous fading. Radiation Protection Dosimetry 17, 493–497. doi: 10.1093/rpd/17.1-4.493.

Thomsen, K.J., Murray, A.S., Jain, M., Bøtter-Jensen, L., 2008. Laboratory fading rates of various luminescence signals from feldspar-rich sediment extracts. Radiation Measurements 43, 1474–1486. doi: 10.1016/j.radmeas.2008.06.002.

Trautmann, T., Krbetschek, M.R., Dietrich, A., Stolz, W., 1998. Investigations of feldspar radioluminescence: potential for a new dating technique. Radiation Measurements 29, 421–425. doi: 10.1016/S1350-4487(98)00012-2.

Trautmann, T., Krbetschek, M.R., Dietrich, A., Stolz, W., 1999. Feldspar radioluminescence: a new dating method and its physical background. Journal of Luminescence 85, 45–58. doi: 10.1016/S0022-2313(99)00152-0.

Valla, P.G., Lowick, S.E., Herman, F., Champagnac, J.D., Steer, P., Guralnik, B., 2016. Exploring $IRSL_{50}$ fading variability in bedrock feldspars and implications for OSL thermochronometry. Quaternary Geochronology 36, 55–66. doi: 10.1016/j.quageo.2016.08.004.

Visocekas, R., 1979. Miscellanous aspects of artificial TL of calcite: emission spectra, athermal detrapping and anomalous fading. PACT 3, 258–265.

Visocekas, R., 1985. Tunnelling radiative recombination in labradorite: its association with anomalous fading of thermoluminescence. Nuclear Tracks 10, 521–529. doi: 10.1016/0735-245X(85)90053-5.

Visocekas, R., 1988. Comparison between tunnelling afterglows following alpha and beta irradiations. Nuclear Tracks and Radiation Measurements 14, 163–168. doi: 10.1016/1359-0189(88)90058-1.

Visocekas, R., Ceva, T., Marti, C., Lefaucheux, F., Robert, M.C., 1976. Tunneling Processes in Afterglow of Calcite. Physica Status Solidi 35, 315–327. doi: 10.1002/pssa.2210350134.

Visocekas, R., Ouchene, M., Gallois, B., 1983. Tunneling afterglow and anomalous fading in dosimetry with $CaSO_4$:Dy. Nuclear Instruments and Methods in Physics Research 214, 553–555. doi: 10.1016/0167-5087(83)90634-8.

Wallinga, J., Murray, A.S., Wintle, A.G., 2000. The single-aliquot regenerative-dose (SAR) protocol applied to coarse-grain feldspar. Radiation Measurements 32, 529–533. doi: 10.1016/S1350-4487(00)00091-3.

Wintle, A.G., 1973. Anomalous fading of Thermoluminescence in Mineral Samples. Nature 245, 143–145. doi: 10.1038/245143a0.

Wintle, A.G., 1977. Detailed study of a thermoluminescent mineral exhibiting anomalous fading. Journal of Luminescence 15, 385–393. doi: 10.1016/0022-2313(77)90037-0.

Wood, R.A., Townsend, P.D., Pells, G.P., Murphy, M.J., 1990. "Anomalous" fading in irradiated α-Al_2O_3. Nuclear Instruments and Methods in Physics Research B 46, 189–193. doi: 10.1016/0168-583X(90)90696-R.

Zink, A.J.C., Visocekas, R., 1997. Datability of sanidine feldspars using the near-infrared TL emission. Radiation Measurements 27, 251–261. doi: 10.1016/S1350-4487(96)00141-2.

Ancient TL

Short Communication

R scripts for dose rate calculation in trapped charge dating

Junjie Zhang[1*], Sumiko Tsukamoto[1,2]

[1]LIAG Institute for Applied Geophysics, Hannover, Germany
[2]Department of Geosciences, University of Tübingen, Tübingen, Germany

*Corresponding author: junjie.zhang@liag-institut.de

Abstract

We present R scripts for environmental dose rate calculations for trapped charge dating, and this contribution introduces these scripts along with associated templates and provides instructions for their use. We also discuss issues related to radon loss and alpha dose rate calculation. In addition to the R scripts for quartz and feldspar, we have prepared R scripts to calculate dose rates of carbonate minerals in a homogeneous medium, and to model the time-dependent changes in dose rates resulting from U-series disequilibrium following carbonate crystallization. These R scripts are freely available on GitHub and Zenodo.

Keywords: Luminescence dating, ESR, Dose rate, R scripts, Radon loss, Alpha efficiency

1. Introduction

To date, a number of programs for dose rate calculation have been developed in trapped charge dating (OSL, TL, and ESR). These include, but are not limited to: ADELE (Degering and Degering, 2020), AGE (Grün, 2009), Carb (Nathan and Mauz, 2008; Mauz and Hoffmann, 2014) and RCarb (Kreutzer et al., 2019), DosiVox (Martin et al., 2015), DRAC (Durcan et al., 2015), DRc (Tsakalos et al., 2015), LDAC (Liang and Forman, 2019) and μRate (Tudyka et al., 2023).

In this short communication, we introduce an alternative approach for dose rate calculation, using code written in the R programming language (R Core Team, 2025). The code and associated files are organized within an R project

named doserate_rProject.Rproj. The main R script used for quartz and feldspar (or polymineral material) is **doserate_main.R**. Two additional R scripts have been prepared for calculating dose rates of carbonate minerals, assuming an infinite homogeneous medium. They are called **doserate_carbonate_keff.R** and **doserate_carbonate_sa.R**. A total of twelve R functions have been developed to support the dose rate calculation process and are utilised by the main R scripts. Unlike some of the previous programs with 'encapsulated' code, these R scripts are more flexible and straightforward to modify, allowing users to easily customise them to suit their specific needs.

2. R scripts for quartz and feldspar

In case of quartz and feldspar (or polymineral material), **doserate_main.R** should be used for dose rate calculation. The flow chart of the calculations is shown in Fig. 1. The R scripts for the functions used for dose rate calculation are stored in the folder 'functions'. The information of the samples should be input into a comma-separated value (CSV) template file: **Template_input.csv**. In the 'mineral' column of the CSV template, either 'fsp' or 'qz' should be entered. The 'fsp' indicates feldspar or polymineral material, and the 'qz' indicates quartz. In the 'grainsize' column of the CSV template, enter either 'coarse' or 'fine'. Here, 'fine' refers to grains between $1\,\mu m$ and $20\,\mu m$ (the 4–11 μm fraction is typically used in dating), while 'coarse' encompasses sizes ranging from $20\,\mu m$ to $1000\,\mu m$. The subdivision of 'fine' and 'coarse' is based on the fact that the grain size related parameters were fitted separately for grains smaller than $20\,\mu m$ and larger than $20\,\mu m$, and different functional scripts for alpha and beta dose rate calculations are applied in the main script.

These grain size related parameters include alpha attenuation factors of U and Th, beta absorption factors of U, Th, K,
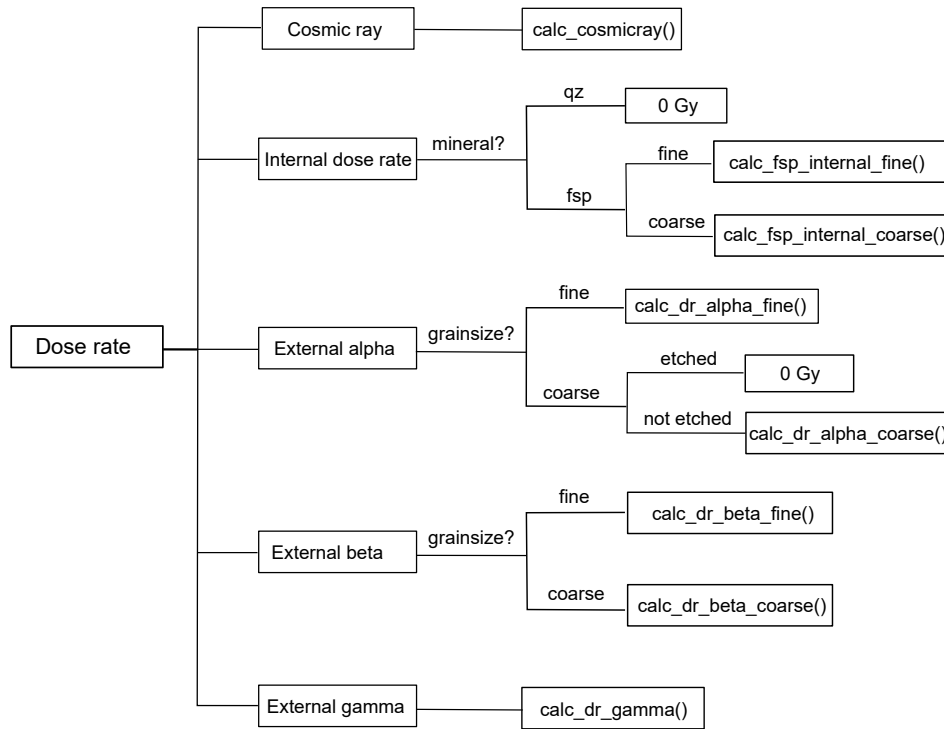
Figure 1: Flowchart of dose rate calculation using the **doserate_main.R** script with defined 'calc_' functional scripts. The parameters 'mineral' and 'grainsize' are entered in the CSV template. For the 'mineral', 'qz' means quartz and 'fsp' means feldspar or polymineral material. For the 'grainsize', 'fine' refers to grains between 1 μm and 20 μm, while 'coarse' refers to grain sizes between 20 μm and 1000 μm.

as well as ^{87}Rb. The alpha attenuation factors used by our R scripts are based on Brennan et al. (1991). The beta absorption factors of U, Th, K are based on Guérin et al. (2012) for grain sizes between 20 μm and 1000 μm, and Brennan (2003) for grain sizes between 1 μm and 20 μm. The absorbed dose for ^{87}Rb beta particles for calculating the internal dose rate of feldspar is based on Readhead (2002). The dose rate contribution of Rb from the external environment is not considered, as it is negligible (e.g., 0.0358 Gy ka^{-1} for 100 μg g^{-1} Rb in a homogeneous medium). The R scripts will calculate these parameters based on the mean grain size, deduced from the 'grain_min' and 'grain_max' values (unit: μm) provided in the CSV file. DRAC applies a smoothed spline function to fit these parameters with the grain size (Durcan et al., 2015). In our R scripts, we use linear and exponential functions for the fitting (see Tables S1–S3 in the Supplementary Materials). Though with different functions, the calculated attenuation or absorption factors from the fittings are always very close to the reported values.

The CSV template includes an 'etch_depth_um' parameter (in μm), which represents the etched thickness, i.e., reduction in grain radius due to HF etching for coarse grains. For fine grains (1–20 μm), the value of zero should always be entered for this parameter. For coarse grains, when the entered value is zero, alpha dose rates will be calculated. When it is greater than zero, alpha dose rates are set to zero with the assumption that the HF etching has sufficiently removed the outer rim affected by alpha irradiation. The en-

tered value will also be used to calculate the etching factor for the beta absorption factor, following the data reported in Brennan (2003) (raw data in the Supplementary Materials of Durcan et al. (2015)). For etched coarse grains, a value of 10 μm is suggested for the 'etch_depth_um' parameter, as reported in previous studies (Bell and Zimmerman, 1978; Porat et al., 2015; Duval et al., 2018).

Other information in the CSV template include: alpha efficiency (a_value), radon loss (Rn_loss), latitude, longitude, altitude (m), burial depth (m), water content (%), U concentration (μg g^{-1}), Th concentration (μg g^{-1}) and K concentration (%), as well as the corresponding errors. Cosmic-ray dose rates are calculated following Prescott and Hutton (1988, 1994). Latitude values should be negative for locations in the southern hemisphere, and longitude values should be negative for locations in the western hemisphere. The default a-value is set to 0.04 ± 0.01 for quartz (e.g., Rees-Jones, 1995; Rees-Jones and Tite, 1997; Lai et al., 2008), and 0.09 ± 0.02 for the pIRIR signal of feldspar (e.g., Kreutzer et al., 2014; Schmidt et al., 2018). For internal dose rate calculation of feldspar, an internal K concentration of 12.5 ± 0.5 % (Huntley and Baril, 1997; Zhao and Li, 2005) and an internal Rb concentration of 400 ± 100 μg g^{-1} (Huntley and Hancock, 2001) are used. These default values can be changed in the 'calc_fsp_internal_coarse' and 'calc_fsp_internal_fine' functional R scripts. Internal dose rates of quartz samples are assumed to be zero. Three sets of conversion coefficients are stored as CSV files in the 'con-

version_data' folder, which are from Guérin et al. (2011), Liritzis et al. (2013) and Cresswell et al. (2018), respectively. Users can choose the conversion coefficients they wish to use by specifying it in the code line of 'conversion <- read.csv()' inside the script **doserate_main.R**. The calculated dose rate results will be saved in the CSV file **Doserate_output.csv**.

2.1. Radon loss

In the gas phase, ^{222}Rn from the ^{238}U decay chain may escape from the sediment matrix, causing disequilibrium in the ^{238}U decay chain (Krbetschek et al., 1994; Olley et al., 1996, 1997). In this case, the dose rates calculated assuming the U series in secular equilibrium will be overestimated. In the R scripts, the ^{238}U decay chain is divided into two segments, pre-Rn and after-Rn. Users can enter any value between 0 and 1 for the 'Rn_loss' parameter in the CSV template. For example, a value of 0 means no Rn loss, and a value of 0.25 means 25 % Rn loss. The degree of Rn loss can be estimated from ^{210}Pb/^{226}Ra activity ratios, in case the samples have been measured by gamma-ray spectrometry (De Corte et al., 2006). We tested the influence of Rn loss on the total dose rates, using sediments from the Rodderberg crater basin, Germany (Zhang et al., 2024b). With a 25 % Rn loss, the dose rates will be 4–5 % lower compared to the dose rate without Rn loss (Fig. 2A).

2.2. Alpha efficiency

Alpha irradiation is less efficient in generating trapped charges (luminescence or ESR signals) than beta and gamma irradiation, per unit of energy deposited. The k-value is defined to describe the alpha efficiency (Zimmerman, 1971), which is equal to the ratio of the beta or gamma dose to the alpha dose that generates the same amount of luminescence. However, by losing the same amount of energy (e.g., 0.1 MeV), an alpha particle with a higher energy (e.g., 4.0 MeV) is more effective than an alpha particle with a lower energy (e.g., 3.0 MeV) in generating luminescence signals. As a result, the k-value will decrease when the alpha particle has a lower energy (Zimmerman, 1971, 1972). The alpha efficiency values were measured using artificial alpha sources, such as ^{210}Po (Zimmerman, 1971, 1972), ^{242}Cm (Aitken and Bowman, 1975), ^{238}Pu (Tribolo et al., 2001), ^{244}Cm (Zhang and Wang, 2020) and ^{241}Am (Mauz et al., 2006; Lai et al., 2008; Biswas et al., 2013; Kreutzer et al., 2014, 2018; Schmidt et al., 2018), which have different alpha energies. In the pioneering work of Zimmerman (1971), the author assumed that all alpha particles emitted by a ^{210}Po source arriving at the sample were mono-energetic at around 3.7 MeV. Hence, the k-value measured by Zimmerman was termed $k_{3.7}$. While the k-value is dependent on the alpha particle's energy, it is found that the luminescence signal produced per unit length of alpha track is nearly independent of the energy (Zimmerman, 1971, 1972; Aitken and Bowman, 1975; Aitken, 1985). Thus, the a-value system was proposed to describe alpha efficiency in terms of generated luminescence per unit track length (Aitken and Bowman, 1975; Aitken, 1985). From the definition of the a-value, it is equal

to $k_{3.7}$ for quartz, and $r \times k_{3.7}$ for other minerals, where r represents the ratio of alpha particle stopping powers between a certain mineral and quartz (Aitken, 1985). According to our calculation, r is 0.98, 1.02 and 1.04 for K-feldspar, calcite and dolomite, respectively (Table S4). Therefore, we can still approximate the a-value as $k_{3.7}$ for these minerals.

In natural environments, the alpha particles received by a fine grain (from U and Th decay chains) have a wide energy spectrum. The average efficiency of these alpha particles in generating luminescence is lower than that of a 3.7 MeV alpha particle (Zimmerman, 1971; Aitken, 1985). Consequently, the effective k-value (k_{eff}) in nature is typically smaller than the $k_{3.7}$ or the a-value. When calculating the natural alpha dose rate, a correction factor should be applied to the a-value or $k_{3.7}$ to obtain the k_{eff}. The correction factors are slightly different between different minerals (Zimmerman, 1971; Aitken, 1985). For quartz, a correction factor of 0.83 was deduced assuming equal U and Th activities (Zimmerman, 1971; Aitken, 1985). It is worth noting that this correction factor is based on TL signals, and such correction factors for OSL and ESR signals have not been reported yet. The correction factors before and after Rn in the decay chain of ^{238}U are also slightly different (Zimmerman, 1971). We have not accounted for the influence of Rn loss on the correction factors, and have applied a constant correction factor of 0.83 in our scripts. If needed, users can change the correction factor in the functional R scripts **calc_dr_alpha_fine.R** and **calc_dr_alpha_coarse.R**, by the parameter of 'a2k' in the code.

Using the a-value to calculate alpha dose rates without converting it to the k_{eff}, the alpha dose rates will be overestimated by ∼20 %. Taking the sediments from the Rodderberg crater basin as an example, alpha dose rates contribute approximately 22 % and 11 % to the total dose rates of fine-grained feldspar and quartz, respectively (Zhang et al., 2024b). Thus, 20 % overestimation in the alpha dose rates will result in 4.4 % and 2.2 % overestimation in the total dose rates for fined-grained feldspar and quartz, respectively (Fig. 2B). In cases where the alpha dose rate makes a major contribution, such as in carbonate rocks, the correction factor from a-value to k_{eff} will be crucial.

2.3. Comparison with DRAC

The dose rates of quartz and feldspar calculated from our R scripts are compared with those calculated by the DRAC software (Durcan et al., 2015). Dose rates were calculated with no Rn loss, as DRAC cannot directly account for Rn loss in its calculation. In the input CSV template of DRAC, we entered the k_{eff} values rather than the a-values. The k_{eff} values were calculated by multiplying a correction factor of 0.83 with the a-values, which are 0.04 ± 0.01 for quartz and 0.09 ± 0.02 for feldspar, respectively. The dose rate results from our R scripts are identical to those from DRAC (Table S5; Fig. 2C).

22

A) Dose rates with 25% Rn loss vs. no Rn loss

B) Dose rates with *a*-value vs. effective *k*-value

C) Dose rates from DRAC vs. R scripts
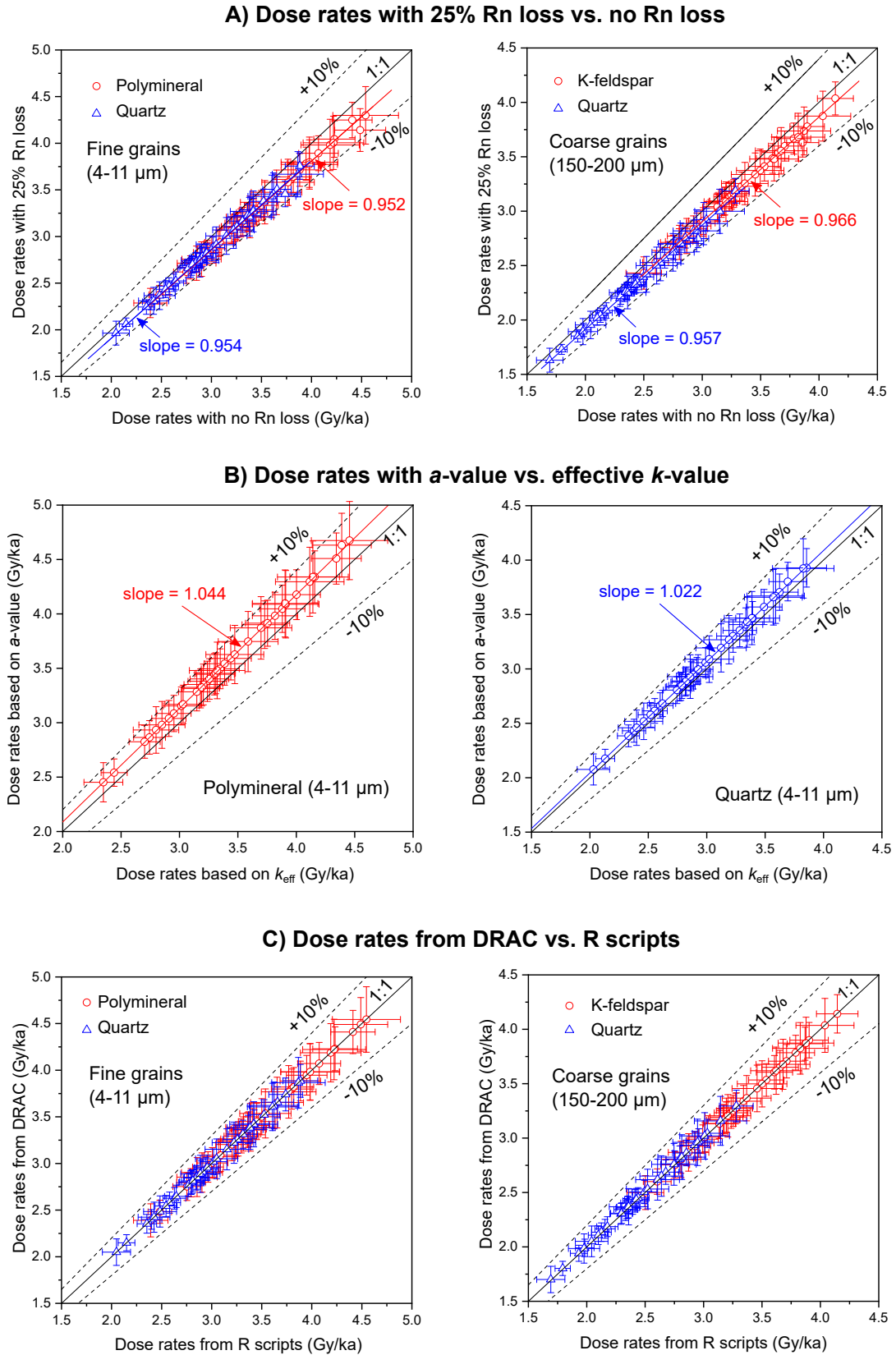
Figure 2: A) Comparison between dose rates calculated with 25 % Rn loss and no Rn loss, for fine grains and coarse grains. B) Comparison between dose rates calculated with the *a*-value and the effective *k*-value (k_{eff}) for fine-grained polymineral material and quartz. C) Comparison between dose rates calculated by DRAC and our R scripts for fine grains and coarse grains. For the coarse grains, the HF etched thickness is set as 10 μm for quartz and 0 μm for K-feldspar. The samples are loess and lacustrine sediments from the Rodderberg crater basin, Germany (Zhang et al., 2024b).

3. R scripts for carbonates

The existing MATLAB[TM] code 'Carb' (Mauz and Hoffmann, 2014) and its translation to R ('RCarb'; Kreutzer et al., 2019) were developed for dose rate calculation of quartz grains inside carbonate rich sediments, to account for the dose rate change with time resulting from the replacement of air and water in the pore space by carbonates. We have prepared two R scripts for dose rate estimation of carbonate minerals in carbonate rocks (e.g., speleothem, limestone, dolostone), using the assumption of an infinite homogeneous medium. These two scripts are **doserate_carbonate_keff.R** and **doserate_carbonate_sa.R**, in the folder named 'doserate_homogeneous_carbonate' under the doserate_rProject. If users apply the effective k-value for the alpha dose rate calculation, the script of **doserate_carbonate_keff.R** should be used in combination with the **Template_carbonate_keff.csv** file. In the template CSV file, users need to enter the k_{eff} values for each individual sample, as alpha efficiency values may vary significantly between different calcite and dolomite samples (e.g., Debenham and Aitken, 1984; Zhang et al., 2025). The alpha dose rate contributes more than 50 % to the total dose rate for carbonate samples in an infinite homogeneous medium (Fig. 3). Therefore, we recommend measuring the alpha efficiency for each individual sample as part of routine procedures in dating carbonates.

In addition to the k-value and a-value systems, the S_α-value system (Guérin and Valladas, 1980) has also been used in calculating the alpha dose rate. With the S_α-value, the effective alpha dose rate can be obtained directly from the alpha flux. If users apply the S_α-value system, the **doserate_carbonate_sa.R** script should be used in combination with the file **Template_carbonate_sa.csv**. S_α-values need to be entered for each sample. The alpha fluxes of $1\,\mu g\,g^{-1}$ (ppm) U or Th in calcite and dolomite are slightly different. In the 'mineral' column of the CSV template, either 'calcite' or 'dolomite' should be entered. The ranges (in $mg\,cm^{-2}$) of alpha particles with different energies for calcite ($\rho = 2.71\,g\,cm^{-3}$) and dolomite ($\rho = 2.85\,g\,cm^{-3}$) were obtained from the software 'The Stopping and Range of Ions in Matter' (SRIM version 2013; Ziegler and Biersack, 1985). With these alpha ranges, the alpha fluxes of $1\,\mu g\,g^{-1}$ U or Th in calcite and dolomite were calculated based on the energy spectrum of emitted alpha particles in their decay chains using an MS Excel[TM] sheet (provided by Norbert Mercier, see Supplementary Materials). For calcite, the alpha fluxes of $1\,\mu g\,g^{-1}$ U and $1\,\mu g\,g^{-1}$ Th are 18,468 and $5,166\,cm^{-2}\,a^{-1}$. For dolomite, the corresponding values are 18,013 and $5,047\,cm^{-2}\,a^{-1}$, respectively. Previous studies have reported alpha ranges for quartz, feldspar and calcite (e.g., Brennan and Lyons, 1989; Valladas, 1988). We have updated these alpha range data with the SRIM 2013 software. Though the ranges of alpha particles are slightly different between different minerals, the alpha fluxes from $1\,\mu g\,g^{-1}$ U or Th differ by less than 3 % between quartz, K-feldspar, calcite and dolomite (see Table S6).

The S_α-value is almost independent of the energy of alpha particles. However, when alpha particle energies fall below 2 MeV, the luminescence generated per unit track length decreases significantly (Zimmerman, 1971, 1972; Aitken and Bowman, 1975; Aitken, 1985). The S_α-values we provide in **Template_carbonate_sa.csv** were measured with an [241]Am source at Archéosciences Bordeaux, CNRS-Université Bordeaux Montaigne (Zhang et al., 2024a, 2025). These values are slightly different from the S_α-values in nature, as the energy spectrum of the alpha particles emitted by the Bordeaux [241]Am source arriving at the aliquots differs from that of the U and Th decay chains in nature (Kreutzer et al., 2018). Correction factors of 0.92 for U and 0.96 for Th have been simulated for the measured S_α-values, respectively (personal communication with Norbert Mercier by email on 29 March 2023). Thus, inside the **doserate_carbonate_sa.R** script, these two correction factors have been multiplied with the S_α-values when calculating alpha dose rates. These correction factors likely differ for different alpha sources used for measuring the S_α-values.

These two R scripts for carbonate dose rate calculation are based on the secular equilibrium state of [238]U. When dating the crystallization event of carbonates (e.g., speleothem growth, shell formation), U-series disequilibrium should be considered. Variation of dose rate through time since carbonate crystallization can be modelled by the **doserate_simulation.R** script in the folder 'correction_for_238U_disequilibrium'. Results are saved as **doserate_simulated_238U_disequilibrium.csv**. The simulation is based on the U concentration and the initial [234]U/[238]U activity ratio. The activities of [238]U, [234]U and [230]Th ($Bq\,kg^{-1}$) are calculated from their decay constants (Fig. 4A). The dose rates from three segments of the [238]U decay chain ([238]U to [234]U, [234]U to [230]Th, [230]Th to [206]Pb) are calculated separately and summed up to obtain the dose rate of the full decay chain (Fig. 4B). Adding the constant dose rates from the [232]Th decay chain, [40]K and cosmic ray, the totally accumulated dose (D_e) with time can be simulated (Fig. 4C). The script **doserate_simulation_for_age_err.R** is used to deduce the age error by the Monte Carlo method. The **age_iteration.R** is another R script to deduce the crystallization age, by an iteration method modified from Ikeya and Ohmura (1983). More details about the modelling can be found in Zhang et al. (2024a).

4. Access to the code and supplementary materials

The R scripts are freely available on GitHub at https://github.com/JunjieZhang113/R-scripts-dose-rate-calculator, and on Zenodo at https://doi.org/10.5281/zenodo.15856401.

Together with the R scripts, supplementary materials are uploaded. These supplementary files include MS Excel[TM] tables showing the fitting of grain size related parameters, the raw data of stopping powers and ranges of alpha particles in different minerals from the SRIM2013 software, and

A) speleothem (LUM4347)

B) dolomite bedrock (LUM4524)

C) loess (LUM4371)

4-11 μm polymineral

4-11 μm quartz
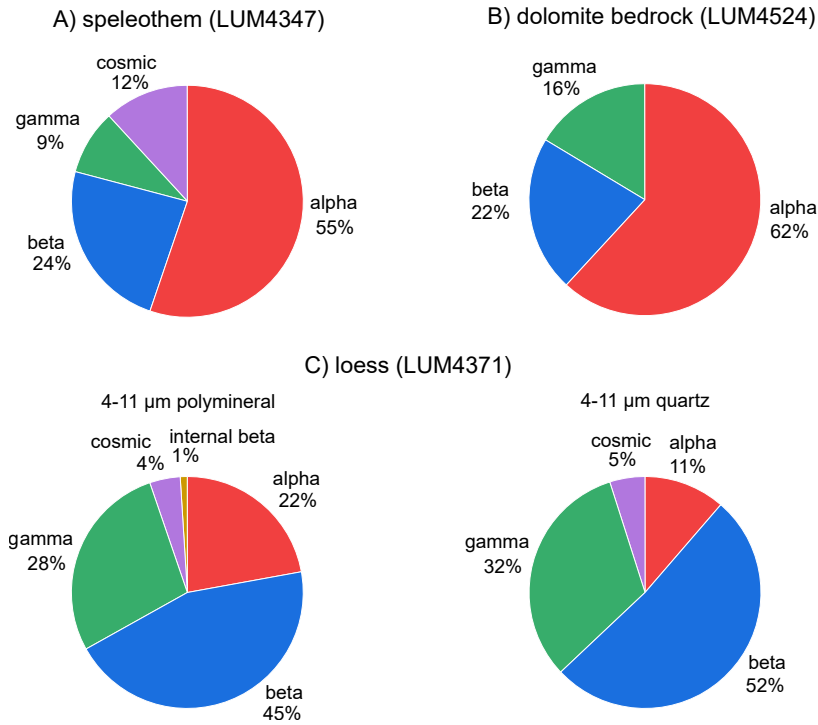
Figure 3: Pie charts showing dose rate compositions of two carbonate samples and one loess sample. A) The speleothem sample is from the Bleßberg cave, Germany (Zhang et al., 2024a). B) The dolomite bedrock sample is from the central Apennines, Italy (Zhang et al., 2025). C) The loess sample is from the Rodderberg crater basin, Germany (Zhang et al., 2024b). Note that for the carbonate samples, alpha dose rates contribute more than half to the total dose rates.

A) Activities with time

B) Dose rate with time

C) D_e with time

$U = 0.67$ μg/g
$[^{234}U/^{238}U]_0 = 2.75$
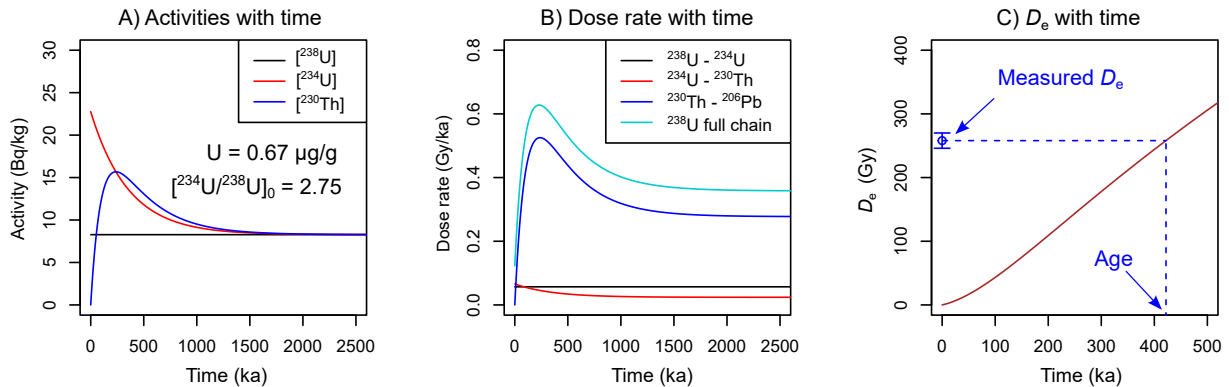
Figure 4: Example for simulating the dose rate change with time since the carbonate crystallization. The sample here is a speleothem (LUM4347) from the Bleßberg cave, Germany (Zhang et al., 2024a).

the summary of alpha fluxes. DRAC dose rate results of the sediment samples from the Rodderberg crater basin are also attached for comparison with dose rate results from the R scripts.

Data availability. All data generated in this study are included in this article, its Supplementary Materials and archived on GitHub and Zenodo.

Conflict of interest. The authors declare that they have no conflict of interest that could have biased their scientific

work.

Review. This article was reviewed by Sebastian Kreutzer.

portunities to measure S_α-values of calcite and dolomite samples at Archéosciences Bodeaux, CNRS-Université Bordeaux Montaigne (France) and the Justus-Liebig University of Giessen (Germany), as well as the discussion about S_α-value evaluation. Norbert Mercier prepared the MS Excel[TM] table to calculate the alpha flux from alpha ranges, and simulated the correction factors for the measured S_α-values to account for the energy spectrum difference between the [241]Am alpha source in Bordeaux and the natural environment. We are grateful to Sebastian Kreutzer whose constructive comments have greatly helped us to improve the manuscript and the R code.

Disclaimer by the reviewer. In 2024, I participated in an extensive scientific discussion via email with the authors and the group in Bordeaux regarding the calculation of the alpha efficiency. Consequently, I was included in the acknowledgements regardless of the provided review. Additionally, during the review process, I recommended incorporating two additional references to this manuscript, where I am the first author (simulation of the [241]Am energy spectrum, RCarb; Kreutzer et al., 2018, 2019). I deem both references relevant to the given context. However, due to my personal bias, it was the authors' prerogative to include them (or not).

Reviewer comment. In my experience with research software development, I have observed over the years that not every newly developed tool is automatically appreciated. Users may be overwhelmed by the abundance of possibilities, leading to confusion about the advantages and disadvantages, and sometimes "yet another tool" mindset. Here, I would like to take the opportunity to highlight three aspects I consider relevant from a research software perspective, underscoring the significance of such contributions. First, through the development of their solution, the authors spent considerable time double-checking existing solutions, thereby verifying and documenting their calculations; a vital aspect of reproducible science. Second, for carbonate and radon loss, they added new code that can be easily used by others, avoiding the need to reinvent the wheel. Lastly, any open-source software alternative is always highly welcome, as it provides users with a choice and allows them to pick their preferred solution.

References

Aitken, M., 1985. Thermoluminescence Dating. Academic Press, London, United Kingdom. doi: 10.1016/C2009-0-06368-8.

Aitken, M.J., Bowman, S.G.E., 1975. Thermoluminescence dating: assessment of alpha particle contribution. Archaeometry 17, 132–138. doi: 10.1111/j.1475-4754.1975.tb00127.x.

Bell, W.T., Zimmerman, D.W., 1978. The effect of HF acid etching on the morphology of quartz inclusions for thermoluminescence dating. Archaeometry 20, 63–65. doi: 10.1111/j.1475-4754.1978.tb00213.x.

Biswas, R.H., Williams, M.A.J., Raj, R., Juyal, N., Singhvi, A.K., 2013. Methodological studies on luminescence dating of volcanic ashes. Quaternary Geochronology 17, 14–25. doi: 10.1016/j.quageo.2013.03.004.

Brennan, B.J., 2003. Beta doses to spherical grains. Radiation Measurements 37, 299–303. doi: 10.1016/S1350-4487(03)00011-8.

Brennan, B.J., Lyons, R.G., 1989. Ranges of alpha particles in various media. Ancient TL 7, 32–37. doi: 10.26034/la.atl.1989.147.

Brennan, B.J., Lyons, R.G., Phillips, S.W., 1991. Attenuation of alpha particle track dose for spherical grains. International Journal of Radiation Applications and Instrumentation. Part D. Tracks Radiation Measurements 18, 249–253. doi: 10.1016/1359-0189(91)90119-3.

Cresswell, A.J., Carter, J., Sanderson, D.C.W., 2018. Dose rate conversion parameters: Assessment of nuclear data. Radiation Measurements 120, 195–201. doi: 10.1016/j.radmeas.2018.02.007.

De Corte, F., Vandenberghe, D., De Wispelaere, A., Buylaert, J.P., Van Den Haute, P., 2006. Radon loss from encapsulated sediments in Ge gamma-ray spectrometry for the annual radiation dose determination in luminescence dating. Czechoslovak Journal of Physics 56, 183–194. doi: 10.1007/s10582-006-1016-3.

Debenham, N.C., Aitken, M.J., 1984. Thermoluminescence dating of stalagmitic calcite. Archaeometry 26, 155–170. doi: 10.1111/j.1475-4754.1984.tb00330.x.

Degering, D., Degering, A., 2020. Change is the only constant - time-dependent dose rates in luminescence dating. Quaternary Geochronology 58, 101074. doi: 10.1016/j.quageo.2020.101074.

Durcan, J.A., King, G.E., Duller, G.A.T., 2015. DRAC: Dose Rate and Age Calculator for trapped charge dating. Quaternary Geochronology 28, 54–61. doi: 10.1016/j.quageo.2015.03.012.

Duval, M., Guilarte, V., Campaña, I., Arnold, L.J., Miguens, L., Iglesias, J., González-Sierra, S., 2018. Quantifying hydrofluoric acid etching of quartz and feldspar coarse grains based on weight loss estimates: implication for ESR and luminescence dating studies. Ancient TL 36, 1–14. doi: 10.26034/la.atl.2018.522.

Grün, R., 2009. "AGE" program for the calculation of luminescence age estimates. Ancient TL 27, 45–46. doi: 10.26034/la.atl.2009.429.

Guérin, G., Mercier, N., Adamiec, G., 2011. Dose-rate conversion factors: update. Ancient TL 29, 5–8. doi: 10.26034/la.atl.2011.443.

Guérin, G., Mercier, N., Nathan, R., Adamiec, G., Lefrais, Y., 2012. On the use of the infinite matrix assumption and associated concepts: A critical review. Radiation Measurements 47, 778–785. doi: 10.1016/j.radmeas.2012.04.004.

Guérin, G., Valladas, G., 1980. Thermoluminescence dating of volcanic plagioclases. Nature 286, 697–699. doi: 10.1038/286697a0.

Huntley, D.J., Baril, M.R., 1997. The K content of the K-feldspars being measured in optical dating or in thermoluminescence dating. Ancient TL 15, 11–13. doi: 10.26034/la.atl.1997.271.

Huntley, D.J., Hancock, R.G.V., 2001. The Rb contents of the K-feldspar grains being measured in optical dating. Ancient TL 19, 43–46. doi: 10.26034/la.atl.2001.333.

Ikeya, M., Ohmura, K., 1983. Comparison of ESR ages of corals from marine terraces with ^{14}C and ^{230}Th/^{234}U ages. Earth and Planetary Science Letters 65, 34–38. doi: 10.1016/0012-821X(83)90187-5.

Krbetschek, M.R., Rieser, U., Zöller, L., Heinicke, J., 1994. Radioactive disequilibria in palaeodosimetric dating of sediments. Radiation Measurements 23, 485–489. doi: 10.1016/1350-4487(94)90083-3.

Kreutzer, S., Martin, L., Dubernet, S., Mercier, N., 2018. The IR-RF alpha-Efficiency of K-feldspar. Radiation Measurements 120, 148–156. doi: 10.1016/j.radmeas.2018.04.019.

Kreutzer, S., Mauz, B., Martin, L., Mercier, N., 2019. 'RCarb': Dose Rate Modelling of Carbonate-Rich Samples - an Implementation of Carb in R. Ancient TL 37, 1–8. doi: 10.26034/la.atl.2019.533.

Kreutzer, S., Schmidt, C., DeWitt, R., Fuchs, M., 2014. The a-value of polymineral fine grain samples measured with the post-IR IRSL protocol. Radiation Measurements 69, 18–29. doi: 10.1016/j.radmeas.2014.04.027.

Lai, Z.P., Zöller, L., Fuchs, M., Brückner, H., 2008. Alpha efficiency determination for OSL of quartz extracted from Chinese loess. Radiation Measurements 43, 767–770. doi: 10.1016/j.radmeas.2008.01.022.

Liang, P., Forman, S.L., 2019. LDAC: An Excel-based program for luminescence equivalent dose and burial age calculations. Ancient TL 37, 21–40. doi: 10.26034/la.atl.2019.536.

Liritzis, I., Stamoulis, K., Papachristodoulou, C., Ioannides, K., 2013. A re-evaluation of radiation dose-rate conversion factors. Mediterranean Archaeology and Archaeometry 13, 1–15.

Martin, L., Incerti, S., Mercier, N., 2015. DosiVox: Implementing Geant 4-based software for dosimetry simulations relevant to luminescence and ESR dating techniques. Ancient TL 33, 1–10. doi: 10.26034/la.atl.2015.484.

Mauz, B., Hoffmann, D., 2014. What to do when carbonate replaced water: Carb, the model for estimating the dose rate of carbonate-rich samples. Ancient TL 32, 24–32. doi: 10.26034/la.atl.2014.481.

Mauz, B., Packman, S.C., Lang, A., 2006. The alpha effectiveness in silt-sized quartz: new data obtained by single and multiple aliquot protocols. Ancient TL 24, 47–52. doi: 10.26034/la.atl.2006.396.

Nathan, R.P., Mauz, B., 2008. On the dose-rate estimate of carbonate-rich sediments for trapped charge dating. Radiation Measurements 43, 14–25. doi: 10.1016/j.radmeas.2007.12.012.

Olley, J.M., Murray, A., Roberts, R.G., 1996. The effects of disequilibria in the uranium and thorium decay chains on burial dose rates in fluvial sediments. Quaternary Science Reviews 15, 751–760. doi: 10.1016/0277-3791(96)00026-1.

Olley, J.M., Roberts, R.G., Murray, A.S., 1997. Disequilibria in the uranium decay series in sedimentary deposits at Allen's cave, nullarbor plain, Australia: Implications for dose rate determinations. Radiation Measurements 27, 433–443. doi: 10.1016/S1350-4487(96)00114-X.

Porat, N., Faerstein, G., Medialdea, A., Murray, A.S., 2015. Re-examination of common extraction and purification methods of quartz and feldspar for luminescence dating. Ancient TL 33, 22–30. doi: 10.26034/la.atl.2015.487.

Prescott, J.R., Hutton, J.T., 1988. Cosmic ray and gamma ray dosimetry for TL and ESR. Nuclear Tracks and Radiation Measurements 14, 223–227. doi: 10.1016/1359-0189(88)90069-6.

Prescott, J.R., Hutton, J.T., 1994. Cosmic ray contributions to dose rates for luminescence and ESR dating: Large depths and long-term time variations. Radiation Measurements 23, 497–500. doi: 10.1016/1350-4487(94)90086-8.

R Core Team, 2025. R: A Language and Environment for Statistical Computing. URL: https://www.R-project.org/. R Foundation for Statistical Computing, Vienna, Austria.

Readhead, M., 2002. Absorbed dose fraction for ^{87}Rb beta particles. Ancient TL 20, 25–28. doi: 10.26034/la.atl.2002.342.

Rees-Jones, J., 1995. Optical dating of young sediments using fine-grain quartz. Ancient TL 13, 9–14. doi: 10.26034/la.atl.1995.242.

Rees-Jones, J., Tite, M.S., 1997. Optical dating results for British archaeological sediments. Archaeometry 39, 177–187. doi: 10.1111/j.1475-4754.1997.tb00797.x.

Schmidt, C., Bösken, J., Kolb, T., 2018. Is there a common alpha-efficiency in polymineral samples measured by various infrared stimulated luminescence protocols? Geochronometria 45, 160–172. doi: 10.1515/geochr-2015-0095.

Tribolo, C., Mercier, N., Valladas, H., 2001. Alpha sensitivity determination in quartzite using an OSL single aliquot procedure. Ancient TL 19, 47–50. doi: 10.26034/la.atl.2001.334.

Tsakalos, E., Christodoulakis, J., Charalambous, L., 2015. The Dose Rate Calculator (DRc) for Luminescence and ESR Dating-a Java Application for Dose Rate and Age Determination. Archaeometry 58, 347–352. doi: 10.1111/arcm.12162.

Tudyka, K., Koruszowic, M., Osadnik, R., Adamiec, G., Moska, P., Szymak, A., Bluszcz, A., Zhang, J., Kolb, T., Poręba, G., 2023. μRate: An online dose rate calculator for trapped charge dating. Archaeometry 65, 423–443. doi: 10.1111/arcm.12828.

Valladas, G., 1988. Stopping power and range for alpha particles in SiO$_2$. Ancient TL 6, 7–8. doi: 10.26034/la.atl.1988.128.

Zhang, J., Arriga, G., Rossetti, F., Argante, V., Kraemer, D., Sontag-González, M., Cosentino, D., Cipollari, P., Tsukamoto, S., 2025. Dolomite luminescence thermochronometry reconstructs the low-temperature exhumation history of carbonate rocks in the central Apennines, Italy. Communications Earth & Environment 6, 252. doi: 10.1038/s43247-025-02216-1.

Zhang, J., Klose, J., Scholz, D., Marwan, N., Breitenbach, S.F.M., Katzschmann, L., Kraemer, D., Tsukamoto, S., 2024a. Isothermal thermoluminescence dating of speleothem growth – A case study from Bleßberg cave 2, Germany. Quaternary Geochronology 85, 101628. doi: 10.1016/j.quageo.2024.101628.

Zhang, J., Wang, L., 2020. Thermoluminescence dating of calcite – Alpha effectiveness and measurement protocols. Journal of Luminescence 223, 117205. doi: 10.1016/j.jlumin.2020.117205.

Zhang, J., Zolitschka, B., Hogrefe, I., Tsukamoto, S., Binot, F., Frechen, M., 2024b. High-resolution luminescence-dated sediment record for the last two glacial-interglacial cycles from Rodderberg, Germany. Quaternary Geochronology 82, 101535. doi: 10.1016/j.quageo.2024.101535.

Zhao, H., Li, S.H., 2005. Internal dose rate to K-feldspar grains from radioactive elements other than potassium. Radiation Measurements 40, 84–93. doi: 10.1016/j.radmeas.2004.11.004.

Ziegler, J.F., Biersack, J.P., 1985. The Stopping and Range of Ions in Matter, in: Bromley, D.A. (Ed.), Treatise on Heavy-Ion Science: Volume 6: Astrophysics, Chemistry, and Condensed Matter. Springer US, Boston, MA, pp. 93–129.

Zimmerman, D.W., 1971. Thermoluminescent Dating Using Fine Grains from Pottery. Archaeometry 13, 29–52. doi: 10.1111/j.1475-4754.1971.tb00028.x.

Zimmerman, D.W., 1972. Relative thermoluminescence effects of alpha- and beta-radiation. Radiation Effects 14, 81–92. doi: 10.1080/00337577208230476.

Thesis Abstracts

Pavlos G. Konstantinidis
Discrimination of different recombination pathways of luminescence in thermoluminescence detectors: optimization over thermal stimulation and detector material

January 2024

Aristotle University of Thessaloniki, Physics Department,
Thessaloniki, Greece

Degree: Ph.D.
Supervisors: Prof. George Kitis, Prof. Alexanda Ioannidou,
Dr. George S. Polymeris

The primary objective of the present doctoral dissertation is to investigate the underlying mechanisms behind the localized and the de-localized recombination pathways during luminescence phenomena, as well as the semi-localized theory. The study begins with an experiment aimed at identifying two main overlapping thermoluminescence (TL) peaks in BeO Radkor, each following different recombination pathways. Thus, a refined protocol is developed to analyse the pathways, using various experimental techniques and heating treatments to distinguish between the two mechanisms.

However, to create the perfect protocol, in addition to BeO Radkor, two more standard dosimetric materials were also used, namely MgB_4O_7:Dy,Na and LiB_4O_7:Cu,In, as it is known from the literature that the first follows the localized pathway, while the second follows the de-localized pathway. The first attempt to create the desired protocol led to a new experimental procedure, which includes techniques like Initial Rise, Peak Shape Methods, and Isothermal Decay, utilizing the Lambert W function. Using this new approach, the activation energies of all the materials were calculated.

To improve the protocol, some modifications were made, including pre-heating treatments of the samples. The second attempt was partially successful, as in the cases of BeO Radkor and MgB_4O_7:Dy,Na, where signs of the transition between the two different recombination pathways were observed. Ultimately, a last modification was made, incorporating both previous protocols and with the help of the final protocol and the use of equations involving the Lambert W function, the desired outcome was achieved: the transition from the localized to the de-localized pathway in the

case of BeO Radkor was observed, strengthening the semi-localized theory. This optimized protocol was also applied to MgB_4O_7:Dy,Na, in which some changes were indeed observed, meaning that a more intense pre-heating treatment could also lead to the transition between the two mechanisms.

The outcome of the dissertation affirms that, with specific thermal treatments and a unique protocol, the semi-localized theory is substantiated, demonstrating the feasibility of transitioning between the two recombination mechanisms.

A PDF of this thesis can be obtained by contacting the author: pavkonst@physics.auth.gr

Anna-Lena Geis
The Chronology of the Riedstadt-Erfelden Drill Core: Application and Comparison of Multi-Method Luminescence Dating

March 2025

Justus-Liebig-University Giessen, Department of Geography,
Giessen, Germany

Degree: M.Sc.
Supervisors: Prof. Dr. Markus Fuchs, Dr. Mariana
Sontag-González

The Upper Rhine Graben is a rift system that contains one of the most continuous sequences of unconsolidated Cenozoic sediments deposited by the river Rhine. Furthermore, its position between the northern European inland and alpine glaciation during the Pleistocene makes it a valuable archive for understanding the interactions of tectonic and climatic control on sedimentation and erosion processes. Thus, numerous drilling projects have been carried out in recent decades. In 2020/21, the Hessian State Agency for Nature Conservation, Environment and Geology (HLNUG) carried out a new continental drilling project near Riedstadt-Erfelden in Hesse, Germany, to obtain further information on the development of the northern Upper Rhine Graben infillings.

This thesis presents new chronological information on the upper section of the core derived from combined luminescence dating approaches. Previously published optically stimulated luminescence (OSL) and infrared radiofluorescence (IR-RF) ages of this core are complemented by recalculated OSL ages due to a new laboratory source calibration and by new measurements using infrared-stimulated luminescence (IRSL), post-infrared-IRSL (pIRIR), and infrared photoluminescence (IRPL). The latter is a novel approach that utilises a potentially non-destructive and non-fading signal from K-feldspar. For the first time, the multiple elevated

temperature (MET)-pIRIR-IRPL single aliquot regenerative dose (SAR) protocol was applied to fluvial samples covering a large age span. Also, a fading test was conducted, and the effect of a varying test dose size was investigated on the signals derived from the protocol.

IRPL ages are in agreement with Middle Pleistocene luminescence ages of previous studies and biostratigraphic and palaeomagnetic data, while showing negligible fading and less sensitivity to a varying test dose size than pIRIR signals. This could be a major advantage of the method. However, IRPL ages overestimate Late Pleistocene quartz OSL ages, an observation that should be investigated further in future studies. Differences in ages between IRPL and IR-RF, although both signals are thought to arise from the same dosimetric trap, could be due to the required differences in sensitivity correction methods. The $pIRIR_{225}$ and $pIRIR_{290}$ ages generally overestimate OSL and IRPL ages, while fading correction of $IRSL_{50}$ ages was not successful, as they still underestimate quartz ages, emphasising the advantages of utilising a potentially non-fading K-feldspar signal. Combined ages indicate a deposition of the Mannheim Formation during the Elsterian-Holsteinian (MIS 11–12) to Weichselian (MIS 2) and a Cromerian (MIS 13–21) age of the Ludwigshafen Formation.

A PDF of this thesis can be obtained by contacting the author: anna-lena.geis@uni-giessen.de.

Aimin Zhang
Quantifying pedoturbation and reconstructing pedogenesis in black soils using single-grain luminescence techniques
June 2025
Chinese Academy of Sciences, Nanjing Institute of Geography and Limnology, Nanjing, China

Degree: Ph.D.
Supervisor: Hao Long

Black soils are vital global "granaries" and terrestrial 'carbon sinks". Studying their age and evolution helps predict future trends and guide conservation efforts. Traditional soil age determination relies on radiocarbon (^{14}C) dating of soil organic matter, but soil's open-system nature leads to mixed-age results. This study approaches the issue from the perspective of soil mineral particles, utilizing single-grain (SG) luminescence dating to characterize the mixing features of black soils and, on this basis, reconstructing its formation process in combination with the deposition history of its parent material.

This study focuses on a black soil profile (GN1) with multiple krotovina (filled animal burrows) in a typical black soil region of Northeast China, as well as four black soil profiles (LS1, SH1, HL5, BA1 from south to north) developed on loess parent material under stable geomorphic conditions across a latitudinal gradient. For each profile, samples for soil property analysis, luminescence dating, and environmental dose rate determination were collected. Basic soil properties — including particle-size distribution, soil organic carbon content, and pH — were measured to characterize the physicochemical characteristics of the profiles. For luminescence dating, quartz and potassium feldspar (K-feldspar) grains were extracted. Both minerals underwent pretest evaluations (e.g., bleaching tests, preheat plateau tests and dose recovery tests) to assess their luminescence characteristics and ensure measurement reliability. Considering testing efficiency, K-feldspar was ultimately selected as the primary material for SG equivalent dose (D_e) determination using the $pIRIR_{225}$ signal.

After comprehensively evaluating the effects of instrumental reproducibility, grain-to-grain variations in luminescence properties, heterogeneous bleaching, and micro-dose rate variations on D_e distributions, the pedoturbation patterns were interpreted. Three indicators—the proportion of zero-dose grains (P_0), overdispersion (OD) of D_e distributions, and the k/p_{max} value derived from the Finite Mixture Model—were used to assess modern downward pedoturbation intensity, overall pedoturbation intensity, and pedoturbation structure, respectively.

To validate the effectiveness of luminescence indicators in characterizing soil mixing, GN1 was analysed by comparing luminescence samples from inside and outside krotovinas. Additionally, regional variations in pedoturbation characteristics were investigated across the four latitudinally distributed black soil profiles. Finally, the formation history of the black soils was reconstructed based on a comprehensive understanding of their soil mixing characteristics. The main findings are as follows:

1. The OD values of single-grain K-feldspar D_e distributions from the five black soil profiles ranged from 21 % to 163 %. Dose-rate analyses and controlled experiments demonstrate that instrumental reproducibility and inter-grain luminescence variations collectively contribute 9–18 % to the OD values, while β-micro-dose-rate heterogeneity accounts for 10–23 %. Heterogeneous bleaching exerts negligible influence. Soil mixing was identified as the dominant factor controlling the dispersion of D_e distributions in the upper horizons of all profiles.

2. The krotovina formation histories of the GN1 profile were reconstructed by comparing intra- and extra-krotovina SG age distributions with depositional contexts. The results indicate that the two black krotovinas (at 80 cm and 160 cm), whose filling materials both mainly originated from the upper soil horizon, were formed during a coeval rapid filling event ≤ 2.7 ka. In contrast, the yellow krotovina at 70 cm was filled with material derived from the lower section of the profile and formed after the initiation of black soil formation.

3. All loess-derived black soil profiles, except the northernmost BA1, contain detectable zero-dose grains.

Within the active mixing zone (defined by maximum zero-dose grain penetration), each profile exhibits coherent decreasing trends in P_0, OD, and k/p_{max} values with depth, demonstrating widespread, depth-dependent weakening of pedoturbation intensity. Spatially, the thickness of the active mixing zone decreases latitudinally from 100 cm (LS1, southernmost) to 35 cm (BA1, northernmost), accompanied by a sharp decline in surface P_0 values from 46–36 % to 3–0 %. These findings reveal a significant northward decrease in soil mixing intensity that correlates well with documented latitudinal patterns of soil faunal activity intensity across Northeast China's black soil region.

4. The deposition age of loess beneath the mollic epipedon (SOC > 6 g kg^{-1}) in profiles LS1, SH1, HL5, and BA1 constrains their black soil ages to no more than 28 ka, 21 ka, 18 ka, and 20 ka, respectively. SH1, HL5, and BA1 retain original depositional signals of the loess parent material within the mollic epipedon, indicating dust accretion during black soil formation, whereas LS1 lacks such signals due to intensive pedoturbation. However, numerical simulations and luminescence profile comparisons under stable versus accreting surface scenarios confirm concurrent dust accretion in LS1 as well. A pronounced mixing intensification marks the onset of black soil formation in LS1 at ∼16 ka.

A PDF of this thesis can be obtained by contacting the author: zhangaimin21@mails.ucas.ac.cn

Bibliography

Compiled by Christoph Schmidt
From 01 December 2024 to 31 May 2025

<u>**Various geological applications**</u>

- aeolian

Bai, X., Zha, X., Huang, C., Zhou, Y., Pang, J., Zhang, Y., Wang, N., Han, Y., 2025. Surface Process and Environment Change Since Last Deglaciation in Western Margin of Zoige Basin, Eastern Tibetan Plateau, China. Chinese Geographical Science 35, 528-544, http://doi.org/10.1007/s11769-025-1513-6

Chen, J., Qiang, M., Wang, X., Xie, J., 2025. Late Quaternary aeolian deposits in the southeastern Mu Us Sandy Land: Insights into the provenance of Asian dust and interpretation of dust records. Quaternary Science Reviews 350, 109168, http://doi.org/10.1016/j.quascirev.2024.109168

Cheng, L., Long, H., Yang, L., Zhang, J., Song, Y., Chen, Z., Wu, Y., Dong, Z., 2025. Mountain glaciers regulate the response of Tibetan Plateau dust activity to global climate change during the last glacial. Quaternary Science Reviews 359, 109375, http://doi.org/10.1016/j.quascirev.2025.109375

Fitzsimmons, K.E., Fischer, M.L., Smith, T., Lauer, T., Nowatzki, M., Mishra, K., Murray-Wallace, C.V., 2025. Long-term hydrologic connectivity on the Australian dryland margins: evidence from the Willandra Lakes World Heritage Area over the last 60 ky. Journal of Quaternary Science. http://doi.org/10.1002/jqs.3717

Mahoney, G., Mandel, R. D., Hanson, P. R., Fritz, S. C., 2025. Early Holocene interaction of aeolian, alluvial, and lacustrine processes in a dune-dammed valley in the central Nebraska Sand Hills. Quaternary Research 124, 121-138, http://doi.org/10.1017/qua.2024.42

- coastal

Cao, Y., Wang, S., Jin, G., Liu, L., Feng, C., Yehia, F., Ma, H., Liu, L., 2025. Enhanced silicate weathering during glacial lowstands: new evidence from shelf sediments in the northern South China Sea. Quaternary Science Advances 18, 100282, http://doi.org/10.1016/j.qsa.2025.100282

Gernant, C., Simms, A. R., DeWitt, R., Theilen, B., Garcia, C. N., Goebel, M., 2025. Insights into the sea-level history of the South Shetland Islands from ground penetrating radar on Livingston Island, Antarctica. Quaternary Science Reviews 359, 109363, http://doi.org/10.1016/j.quascirev.2025.109363

Liu, Y., Wu, Z., Long, G., Feng, X., Lai, P., Fang, Z., Wu, W., Xu, J., Xu, G., Tu, H., Li, H., Wang, W., Lai, Z., 2025. Response to sea-level change in a non-deltaic coastal plain: Insights from cores chronologies. Geomorphology 476, 109678, http://doi.org/10.1016/j.geomorph.2025.109678

Martins, A. A., Gouveia, M. P., Cunha, P. P., Cabral, J., Gomes, A., Falguères, C., Voinchet, P., Stokes, M., Caldeira, B., Buylaert, J.-P., Murray, A. S., Bahain, J.-J., Figueiredo, S., 2025. Marine terrace staircases of western Iberia: Uplift rate patterns from rocky limestone coasts of central Portugal (Cape Raso - Abano beach and Cape Espichel). Quaternary International 720, 109657, http://doi.org/10.1016/j.quaint.2024.109657

Perazzotti, F., Valle, L. d., Cossu, G., Pascucci, V., Fornós, J. J., 2025. Paleoenvironmental changes and sea-level fluctuations record at Punta de s'Avançada, Mallorca Island. Quaternary International 735, 109839, http://doi.org/10.1016/j.quaint.2025.109839

Wang, Q., Zhan, C., Su, T., Shi, H., Wang, L., Zeng, L., Liu, X., Cui, B., 2025. Causes and Geomorphological Effects of Relative Sea Level Movement in the Yellow River Delta During the Last 2000 Years. Journal of Ocean University of China 24, 323-331, http://doi.org/10.1007/s11802-025-5882-3

Wang, Y., Meltzner, A. J., Quye-Sawyer, J., Yang, H., Pu, Y., Qin, J., Aung, L. T., Aw, Z., Pamintuan, A. D. A., Ramos, N. T., 2025. Uplift, tilting, and underlying structures of coastal northwestern Luzon, Philippines, deduced from marine terraces. Quaternary Science Reviews 358, 109347, http://doi.org/10.1016/j.quascirev.2025.109347

- colluvial

Riedesel, S., Guérin, G., Thomsen, K. J., Sontag-González, M., Blessing, M., Botha, G. A., Hellers, M., Möller, G., Peffeköver, A., Sommer, C., Zander, A., Will, M., 2025. A direct comparison of single-grain and multi-grain aliquot luminescence dating of feldspars from colluvial deposits in KwaZulu-Natal, South Africa. Geochronology 7, 59-81, http://doi.org/10.5194/gchron-7-59-2025

- earthquakes and tectonic activity

Cholponbek, O., Ha, S., Seong, Y. B., Sultan, B., Erkin, R., Mirlan, D., Sanzhar, S., 2025. Issyk-Ata fault and its two strong Holocene paleoearthquakes records near densely populated Chui basin: focus on Dzhal area of Kyrgyz Range, Tien Shan. Journal of Mountain Science 22, 404-421, http://doi.org/10.1007/s11629-024-9145-3

Escuder-Viruete, J., Fernández, F. J., Valera, F. P., Medialdea, A., Castillo-Carrión, M., 2025. Present-Day Shortening Accommodated by Folding, Thrusting and Strike-Slip Faulting in the Enriquillo Basin of Southern Central Hispaniola: Implications for the Regional Seismic Hazard. Tectonics 44, e2024TC008376, http://doi.org/10.1029/2024TC008376

Gonzalez, G., Astudillo-Sotomayor, L., Del Rio, I., Sawakuchi, A. O., Amidon, W., 2025. Tracing the relationship between the upper plate earthquake cycle and megathrust slip, the Atacama fault system in Northern Chile. Scientific Reports 15, 2914, http://doi.org/10.1038/s41598-025-86877-0

Gegg, L., Moine, O., Stojakowits, P., Preusser, F., 2025. Sediment dynamics, neotectonic activity and palaeoenvironments recorded in the Quaternary infill of the central Upper Rhine Graben. Quaternary Science Advances 18, 100284, http://doi.org/10.1016/j.qsa.2025.100284

Hu, X., Yi, Z., Chen, J., Zhang, Y., 2025. Kinematics and deformation rates of the fault-fold system along the eastern section of the North Qilian Shan Fault. Science China Earth Sciences 68, 1326-1345, http://doi.org/10.1007/s11430-024-1478-7

Hu, Z., Li, A., Yuan, H., Zuo, Y., Yang, X., Yang, H., 2025. The Tuoli Fault: Late Pleistocene Tectonics and Slip Rate of a Left-Lateral Strike-Slip Fault in the Western Junggar Mountains, NW China. Tectonics 44, e2025TC008820, http://doi.org/10.1029/2025TC008820

John, B., Singh, Y., Rajendran, C. P., 2025. Sedimentary records of liquefaction from central Kerala (southwestern India), as earthquake indicators in a cratonic area. Journal of Asian Earth Sciences 277, 106373, http://doi.org/10.1016/j.jseaes.2024.106373

Lei, X., Liang, K., Ma, B., He, Z., Wang, J., Zhao, J., Guan, Y., 2025. Vertical Slip Rate and Tectonic Context of the Langshan Piedmont Fault, Northwestern Ordos Area, China. Tectonics 44, e2024TC008442, http://doi.org/10.1029/2024TC008442

Li, L.-W., Yu, Z.-Y., Qiu, C.-M., Wang, W.-X., Zhao, Q., Zheng, R.-Y., Yang, Y.-L., 2025. Late Quaternary slip rate of the Northern Margin Fault of the Huaizhuo Basin in the North China Block and its seismological implications. Applied Geophysics 22, 53-70, http://doi.org/10.1007/s11770-025-1171-6

Liu, J., Ren, Z., Nissen, E., Zhang, C., Li, Z., Zhang, Z., Wu, D., 2025. Spatially Variable, Multi-Mm/Yr Late Pleistocene-Holocene Slip Rates Along the South Riyueshan Fault Highlight Limitations to Block-Like Behavior in the NE Tibetan Plateau, China. Tectonics 44, e2024TC008562, http://doi.org/10.1029/2024TC008562

Ocakoğlu, F., Tün, M., Şahiner, E., 2025. Early Pleistocene initiation of Simav Graben: Implications for widespread extension and landscape change in West Anatolia. Earth Surface Processes and Landforms 50, e6060, http://doi.org/10.1002/esp.6060

Shtober-Zisu, N., Kranenburg, H., Waldmann, N., Porat, N., Shaar, R., Brook, A., Greenbaum, N., 2025. Tectono-sedimentary evolution of a marginal fault: Insights from the Dead Sea Transform Fault System. Quaternary International 718, 109637, http://doi.org/10.1016/j.quaint.2024.109637

Wang, D., Chen, L., Chang, H., Kang, S., Jia, Y., Du, J., Han, F., Li, Y., Yin, G., Zheng, W., Wang, X., 2025. Late Quaternary vertical throw rates along the Gyaring Co fault in central Tibet. Journal of Asian Earth Sciences 280, 106484, http://doi.org/10.1016/j.jseaes.2024.106484

Xie, C., Li, W., Liu, X., Dang, H., Huang, Y., Long, P., 2025. Paleoearthquakes along the northeastern segment of the Yabrai range-front fault in the Alashan Block, northeast of the Tibetan Plateau. Journal of Quaternary Science 40, 372-384, http://doi.org/10.1002/jqs.3690

Yang, H., Lin, D., Yang, X., Cunningham, D., Hu, Z., Huang, X., Zhang, Y., Li, A., 2024. Strain Partitioning and Strike-Slip Faulting in the Nanjieshan, North Tibetan Foreland: Progressive Widening of the Altyn Tagh Fault System With Implications for Regional Earthquake Hazards. Tectonics 43, e2024TC008262, http://doi.org/10.1029/2024TC008262

- fluvial

Antinao, J. L., Maldonado, A., Díaz, L., Negrini, R. M., Tiner, R., Flores-Aqueveque, V., Moreiras, S. M., Brown, N., McDonald, E., 2025. Late Quaternary alluvial fan stratigraphy and chronology, Elqui, Turbio and Claro valleys, semiarid Andes of Chile. Quaternary International 727, 109765, http://doi.org/10.1016/j.quaint.2025.109765

Bertran, P., Andrieux, E., Leleu, S., Sicard-Delage, Z., Fores, B., Ouchaou, R., Weill, P., Reynaud, J.-Y., 2025. The Late Pleistocene - Holocene meandering lower Garonne River, southwest France: Architecture of the valley fill and chronology, comparison with other European rivers. Geomorphology 468, 109469, http://doi.org/10.1016/j.geomorph.2024.109469

D'Arcy, M. K., Schildgen, T. F., Bonnet, S., Duesing, W., Tofelde, S., Roda-Boluda, D. C., Wittmann, H., Mey, J., Murray, A. S., Alonso, R. N., Strecker, M. R., 2025. A 300 kyr record of past hydroclimate change from alluvial fans in the southern Central Andes. Earth Surface Processes and Landforms 50, e70006, http://doi.org/10.1002/esp.70006

Duan, M., Neubauer, F., Robl, J., Zhou, X., Argentin, A.-L., Liebl, M., Dong, Y., Shi, X., Zhang, S., Peng, H., 2025. The northward expansion of the Tibetan Plateau: Topographic evidence from the Bogda Mts. – southern Junggar Basin coupling system, northwest China. Quaternary Science Reviews 362, 109402, http://doi.org/10.1016/j.quascirev.2025.109402

Fülling, A., Graf, H. R., Hofmann, F. M., Mueller, D., Preusser, F., 2024. Age and formation of the presumed Late Pliocene to Middle Pleistocene Mühlbach formation, High Rhine Valley, southwest Germany. E&G Quaternary Sci. J. 73, 203-216, http://doi.org/10.5194/egqsj-73-203-2024

Gallen, S. F., Wegmann, K. W., 2025. The impact of river capture on fluvial terraces and bedrock incision. Earth Surface Processes and Landforms 50, e70035, http://doi.org/10.1002/esp.70035

Hou, R., Wu, M., Chen, N., Wu, K., Chen, X., She, D., Huang, N., Xiao, M., 2025. Human settlements lie on paleolandslide deposits:Risk, evidence and formation of an ancient river-blocking landslide in the Jinsha River tributary, SE Tibetan Plateau. CATENA 249, 108664, http://doi.org/10.1016/j.catena.2024.108664

Hu, G., Hu, C., Wu, X., Pan, G., Zhuma, D., He, Q., Wang, H., Wang, P., Xu, L., Xie, J., Zhang, J., Wang, X., Tang, Y., 2025. Fluvial downcutting and its influence on human settlement in the middle reaches of the Lancang River. Geomorphology 477, 109703, http://doi.org/10.1016/j.geomorph.2025.109703

Hu, X., Yi, Z., Chen, J., Zhang, Y., 2025. Kinematics and deformation rates of the fault-fold system along the eastern section of the North Qilian Shan Fault. Science China Earth Sciences 68, 1326-1345, http://doi.org/10.1007/s11430-024-1478-7

Karakoca, E., Uncu, L., Sarikaya, M. A., Şahiner, E., Köse, O., 2025. Geomorphology and chronology of Late Quaternary terrace staircases of the Sakarya River, northwest Türkiye. Journal of Quaternary Science 40, 386-399, http://doi.org/10.1002/jqs.3695

Langston, A. L., Marcotte, A. L., Neudorf, C. M., Rodrigues, K., Keen-Zebert, A., 2025. Interpreting depositional environments from modern floodplain sediments using optically stimulated luminescence. Boreas 54, 14-33, http://doi.org/10.1111/bor.12679

Li, Z.-K., Li, S.-H., Li, Y.-L., 2025. The large distribution of inverted stream channel terrains in the western Qaidam Basin, North Tibetan Plateau, and implications to the fluvial ridges on Mars. Geomorphology 473, 109632, http://doi.org/10.1016/j.geomorph.2025.109632

Liao, Y., Lu, P., Mo, D., Wu, Q., Zhao, X., Li, Y., Chen, P., Wang, H., 2025. Landscape evolution and ancient settlement patterns in a small river basin of the Huangshui River and the prehistoric Wangjinglou City, Central China. Quaternary Research 124, 94-104, http://doi.org/10.1017/qua.2024.45

Ma, Y., Li, Z., Tan, D., Zou, X., Tao, T., 2025. Rare earth element characteristics of Holocene sediments at the southern margin of the Gurbantunggut Desert and their implications for provenance. Earth Surface Processes and Landforms 50, e70022, http://doi.org/10.1002/esp.70022

Mahadev, Behera, D., Kumar, P., Jaiswal, M. K., Singh, A. K., 2025. A Terrestrial record of ~3000 years of extreme floods from the Kaveri and adjacent river basins, Tamil Nadu, India. Quaternary International 738, 109856, http://doi.org/10.1016/j.quaint.2025.109856

Nogueira, A. M., Caldeira, D., Uagoda, R., Mendes, L. C., 2025. The Pleistocene-Holocene history of a fluviokarst landscape in Central Brazil: An analysis of the river sediments of the Extrema, das Pedras and Ventura dry valleys. Quaternary International 725-726, 109735, http://doi.org/10.1016/j.quaint.2025.109735

Parida, S., Kaushal, R. K., Chauhan, N., Singhvi, A. K., 2025. Changes in thermoluminescence sensitivity of 110°C glow peak of quartz grains from sediments of River Ganga: Observation and implications. Earth and Planetary Science Letters 656, 119267, http://doi.org/10.1016/j.epsl.2025.119267

Qian, H., Jiang, X., Chen, H., Mi, R., Lash, G. G., Li, H., 2025. River terraces along the Liujiang River in Southwest China and their implications for understanding fluvial processes on the Guizhou Plateau since the Late Pleistocene. Quaternary Research 125, 118-133, http://doi.org/10.1017/qua.2024.44

Roberto Pinheiro, M., Mateus Barreiros, A., Bungenstab Alves, G., Reis Nakashima, M., Ferraz Scigliano, B., Filipe Amaral Soares, A., Artur dos Santos, A., Renata Guimarães Borsoi, H., Carlos de Azevedo, A., N Pupim, F., Breda, C., Nadal Junqueira Villela, F., 2025. Origin of surface deposits in pediments of Southeastern Brazil. CATENA 249, 108642, http://doi.org/10.1016/j.catena.2024.108642

Shang, L., Zha, X., Huang, C., Zhou, Y., Pang, J., Li, Y., Wang, Z., 2025. Reconstructing the magnitudes of Holocene extraordinary floods in the upper Huai River, China. Quaternary Science Reviews 359, 109371, http://doi.org/10.1016/j.quascirev.2025.109371

Srisunthon, P., Abdulkarim, M., Berger, A., Ertlen, D., Fülling, A., Kirch, L., Mueller, D., Reubold, M., Preusser, F., 2025. First insights into the Late Quaternary fluvial history of the Nan River, northern Thailand. Environmental Earth Sciences 84, 268, http://doi.org/10.1007/s12665-025-12243-y

Tanski, N. M., Pederson, J. L., Hidy, A. J., Rittenour, T. M., Mauch, J. P., 2025. The Mystery of Baselevel Controls in the Incision History of the Central Colorado Plateau. AGU Advances 6, e2024AV001359, http://doi.org/10.1029/2024AV001359

Zhang, Y., Hu, X., Cao, X., Yi, Z., Ren, Q., Deng, X., 2025. Tectonic uplift recorded by the river terraces in the northern flank of East Kunlun Shan. Geomorphology 476, 109677, http://doi.org/10.1016/j.geomorph.2025.109677

Zvara, E., Pejdanovic, S., Schneider, B., Quante, E., Saeidi ghavi andam, S., Volosky, D., Lauer, T., Fitzsimmons, K.E., Marhan, S., Kandeler, E., Poll, C., Oelmann, Y., Neidhardt, H., Lindauer, S., Friedrich, R., Werther, L., Frenzel, P., Kühn, P., Zielhofer, C., 2025. Biochemostratigraphy of the Eger floodplain – detection and quantification of heavy metal contamination and palaeoenvironmental conditions: the basic dataset. Data in Brief 60, 111501, http://doi.org/10.1016/j.dib.2025.111501

- glacial and periglacial

Bai, X., Zha, X., Huang, C., Zhou, Y., Pang, J., Zhang, Y., Wang, N., Han, Y., 2025. Surface Process and Environment Change Since Last Deglaciation in Western Margin of Zoige Basin, Eastern Tibetan Plateau, China. Chinese Geographical Science 35, 528-544, http://doi.org/10.1007/s11769-025-1513-6

Bateman, M. D., Davies, E., Evans, D. J. A., Roberts, D. H., Connell, E. R., Rhodes, E. J., 2025. Developing a new approach to the luminescence dating of sediments from glacial contexts. Quaternary Geochronology 87, 101659, http://doi.org/10.1016/j.quageo.2025.101659

Kalińska, E., Weckwerth, P., Alexanderson, H., Piotrowski, J. A., Wysota, W., 2025. OSL dating of glacial outburst flood deposits in NE Poland and their bleaching problem inferred from the landform-sediment associations and regional context. Quaternary Research 124, 26-46, http://doi.org/10.1017/qua.2024.50

Krauß, N., Börner, A., Kenzler, M., 2025. Geochronological investigations at the maximum extent of the Fennoscandian Ice Sheet during the Late Weichselian glaciation in northern Germany. Boreas 54, 246-257, http://doi.org/10.1111/bor.12695

Murton, J. B., Opel, T., Toms, P., Wood, J., Boxleitner, K., Savvinov, G., Danilov, P., Boeskorov, V., Goslar, T., Rogers, G., Lupachev, A., Tikhonravova, Y., 2025. Preliminary paleoenvironmental analysis and luminescence dating of upper Middle Pleistocene permafrost deposits of the Ulakhan Sular Formation, Adycha River, east Siberia. Quaternary Research 124, 1-25, http://doi.org/10.1017/qua.2024.36

Penprase, S. B., Wickert, A. D., Larson, P. H., Wood, J. J., Larsen, I. J., Rittenour, T. M., 2025. Plow versus Ice Age: Erosion rate variability from glacial–interglacial climate change is an order of magnitude lower than agricultural erosion in the Upper Mississippi River Valley, USA. Geology 53, 535-539, http://doi.org/10.1130/g52585.1

Serra, E., Mueller, D., Gegg, L., Firla, G., Piccoli, F., Hergarten, S., Margirier, A., Preusser, F., 2025. Combined single grain and cobble luminescence dating of poorly bleached glaciofluvial deposits from the Swiss Alpine foreland. Quaternary Geochronology 87, 101650, http://doi.org/10.1016/j.quageo.2025.101650

Wilcox, P. S., Meyer, M. C., Festi, D., 2025. Semi-continuous release of Cordilleran Ice Sheet meltwater between 20,000 and 17,000 years ago. Nature Geoscience 18, 459-461, http://doi.org/10.1038/s41561025-01694-4

- lacustrine

Ataee, N., Roberts, H. M., Duller, G. A. T., 2025. Assessing the potential of a modified post-isothermal IRSL (pIt-IR) protocol to circumvent the problems posed by anomalous fading in polymineral fine grains. Quaternary Geochronology 88, 101676, http://doi.org/10.1016/j.quageo.2025.101676

Chahal, P., Matmon, A., Porat, N., Paudayal, K. N., Goldsmith, Y., 2025. The Rise and Fall of Marpha Lake, a Late Quaternary Dammed Lake in the Himalayan Rain-Shadow With Implications to Landscape Evolution and Sediment Dynamics. Journal of Geophysical Research: Earth Surface 130, e2024JF007959, http://doi.org/10.1029/2024JF007959

Fitzsimmons, K.E., Fischer, M.L., Smith, T., Lauer, T., Nowatzki, M., Mishra, K., Murray-Wallace, C.V. (2025) Long-term hydrologic connectivity on the Australian dryland margins: evidence from the Willandra Lakes World Heritage Area over the last 60 ky. Journal of Quaternary Science, http://doi.org/10.1002/jqs.3717

Hu, F., Xiao, X., Fan, Q., Yu, L., Xu, Y., Feng, Y., Zhou, Y., Yu, M., 2025. Grain size and shape analysis of recent and paleo sediments along Poyang Lake with insight into its environmental significance. CATENA 248, 108588, http://doi.org/10.1016/j.catena.2024.108588

Mahoney, G., Mandel, R. D., Hanson, P. R., Fritz, S. C., 2025. Early Holocene interaction of aeolian, alluvial, and lacustrine processes in a dune-dammed valley in the central Nebraska Sand Hills. Quaternary Research 124, 121-138, http://doi.org/10.1017/qua.2024.42

Wolf, D., Lehmkuhl, F., Schaubert, V., Rahimzadeh, N., Frechen, M., Stauch, G., Batkhishig, O., Wegmann, K., 2025. Drivers of late Quaternary lake level fluctuations of Khyargas Nuur, western Mongolia - glacial meltwater discharge or atmospheric moisture supply? Quaternary Science Reviews 359, 109373, http://doi.org/10.1016/j.quascirev.2025.109373

Yang, A., Liu, W., Wang, H., Hu, K., Li, X., Cong, L., Zhou, Y., Yang, Z., 2025. Dammed lake chronology in the middle Yarlung Tsangpo River: Tracing the origin of late Holocene megafloods. Quaternary Science Reviews 350, 109155, http://doi.org/10.1016/j.quascirev.2024.109155

- landslide

Chalupa, V., Pánek, T., Břežný, M., Gutiérrez, F., Medialdea, A., 2025. Evolution of deep-seated gravitational slope deformation in a deep valley of the Czech Flysch Carpathians. Geomorphology 470, 109545, http://doi.org/10.1016/j.geomorph.2024.109545

Hou, R., Wu, M., Chen, N., Wu, K., Chen, X., She, D., Huang, N., Xiao, M., 2025. Human settlements lie on paleolandslide deposits: Risk, evidence and formation of an ancient river-blocking landslide in the Jinsha River tributary, SE Tibetan Plateau. CATENA 249, 108664, http://doi.org/10.1016/j.catena.2024.108664

Nikolaeva, S. B., Tolstobrov, D. S., 2025. Gravity Flows in Late Quaternary Sediments in Northwestern Russia (Kola Region) and Their Possible Relationship with Pleistocene Earthquakes. Lithology and Mineral Resources 60, 43-57, http://doi.org/10.1134/S0024490224700822

- loess

Amiri, Z., Khormali, F., Kehl, M., Frechen, M., Zeeden, C., 2025. Pedogenesis and paleoenvironmental reconstruction in northern Iran: The loess-paleosol sequence at Baluchabad. CATENA 253, 108835, http://doi.org/10.1016/j.catena.2025.108835

Constantin, D., Begy, R., Vandenberghe, D. A. G. J., Veres, D., Timar-Gabor, A., 2025. An empirical study on the variability of luminescence ages for coeval sediment samples. Radiation Measurements 182, 107401, http://doi.org/10.1016/j.radmeas.2025.107401

Gao, Z., Wang, Z., Wang, Y., Zhang, Z., Cao, M., Kemp, D. B., 2024. Regional differences in millennial-scale climate variability in northeastern Tibet loess deposits spanning 34 ka to 8 ka. GSA Bulletin 137, 2407-2414, http://doi.org/10.1130/b37931.1

Kittel, P., Makohonienko, M., Apolinarska, K., Golyeva, A., Okupny, D., Ginter, A., Borówka, R. K., Rennwanz, J., Kramkowski, M., Poręba, G., Szymak, A., Pokutta, D., Sîrbu, G., Rybicka, M., 2025. A comprehensive palaeoecological study of humic deposits and loess profiles as a tool for understanding past human-environmental relationships at Tripolye Culture Gordineşti II-Stînca goală site, Northern Moldova. Journal of Archaeological Science: Reports 62, 105057, http://doi.org/10.1016/j.jasrep.2025.105057

Li, D., Zhao, H., Xie, H., Sun, A., Khormali, F., Wang, X., Wang, Q., Lahijani, H., Nashli, H. F., Xu, Y., Chen, F., 2025. Loess-paleosol sedimentological characteristics in northern Iran since the last interglacial and their paleoenvironmental significance. Quaternary Science Reviews 354, 109213, http://doi.org/10.1016/j.quascirev.2025.109213

Liu, L., Yang, S., Li, P., Zhang, J., Li, R., Li, D., Xu, X., Luo, Y., Yang, X., 2025. First investigation of the luminescence dating of loess in the eastern Tibetan Plateau using K-feldspar MAR MET-pIRIR protocol. Quaternary Geochronology 86, 101648, http://doi.org/10.1016/j.quageo.2024.101648

Perić, Z. M., Radaković, M. G., Marković, R. S., Marković, S. B., 2025. A synthesis of luminescence and 14C dated dust mass accumulation rates for loess-palaeosol sequences from the Middle Danube Basin. Boreas 54, 179-201, http://doi.org/10.1111/bor.12696

Shu, P., Zhou, W., Putnam, A. E., Li, B., Kang, S., Sha, Y., Shi, Z., Ming, G., Wang, H., Sun, Y., Wright, D. K., Liu, W., Liu, X., Cheng, P., Song, Y., Niu, D., Dodson, J. R., Du, H., Zhao, J., Zhang, Z., Qiu, Y., An, Z., 2025. Intensified monsoonal rainstorm events over westerly-dominated Asian interior during the warm mid-Holocene. Communications Earth & Environment 6, 72, http://doi.org/10.1038/s43247-025-02005-w

Vandenberghe, J., Vandenberghe, D. A. G., Huijzer, A. S., De Grave, J., 2025. Loess facies analysis and chronology to reconstruct morpho-sedimentary and palaeoclimatic evolution: A case study from the

Belgian-Dutch Maas valley. Quaternary Science Reviews 352, 109163, http://doi.org/10.1016/j.quascirev.2024.109163

- provenance

Campos, M. C., Chiessi, C. M., Nascimento, R. A., Kraft, L., Radionovskaya, S., Skinner, L., Dias, B. B., Pinho, T. M. L., Kochhann, M. V. L., Crivellari, S., Mineli, T. D., Mendes, V. R., Baker, P. A., Silva, C. G., Sawakuchi, A. O., 2025. Millennial- to centennial-scale Atlantic ITCZ swings during the penultimate deglaciation. Quaternary Science Reviews 348, 109095, http://doi.org/10.1016/j.quascirev.2024.109095

Liu, Y., Wu, Z., Long, G., Feng, X., Lai, P., Fang, Z., Wu, W., Xu, J., Xu, G., Tu, H., Li, H., Wang, W., Lai, Z., 2025. Response to sea-level change in a non-deltaic coastal plain: Insights from cores chronologies. Geomorphology 476, 109678, http://doi.org/10.1016/j.geomorph.2025.109678

Ma, Y., Li, Z., Tan, D., Zou, X., Tao, T., 2025. Rare earth element characteristics of Holocene sediments at the southern margin of the Gurbantunggut Desert and their implications for provenance. Earth Surface Processes and Landforms 50, e70022, http://doi.org/10.1002/esp.70022

Parida, S., Kaushal, R. K., Chauhan, N., Singhvi, A. K., 2025. Changes in thermoluminescence sensitivity of 110°C glow peak of quartz grains from sediments of River Ganga: Observation and implications. Earth and Planetary Science Letters 656, 119267, http://doi.org/10.1016/j.epsl.2025.119267

- soil

Ganzawa, Y., Katsumi, N., Ito, H., Mitsuzawa, G., Shimizu, M., 2025. Weathering Effects on Luminescence Dating – An Example of the Toya Tephra in Japan. Island Arc 34, e70010, http://doi.org/10.1111/iar.70010

Holmer, A. S., Bősze, I., Moosbauer, G., Lindauer, S., Völkel, J., 2025. Neolithic formation of chernozem in south-eastern Germany? CATENA 248, 108543, http://doi.org/10.1016/j.catena.2024.108543

Kapur, S., Akça, E., Kadir, S., Previtali, F., Billor, Z., Zucca, C., Casati, E., Eren, M., Karagöz, A., Nazik, A., Berberoğlu, S., Özberk, İ., Yeğingil, Z., Polat, O., Madrau, S., Zoroğlu, L., Dönmez, C., Çilek, A., 2025. Pedogenic evidence sheds light on the post-Roman pedo-sedimentological and human history of Tarsus, the Roman capital of CE 60, Cilicia, Mersin, Türkiye. CATENA 248, 108544, http://doi.org/10.1016/j.catena.2024.108544

Panin, P., Kalinin, P., Konstantinov, E., Sychev, N., 2025. New data on the MIS 5e paleosol found in the loess-paleosol sequence of the Elista section (Republic of Kalmykia). CATENA 250, 108745, http://doi.org/10.1016/j.catena.2025.108745

van der Meij, W. M., Riedesel, S., Reimann, T., 2025. Mixed Signals: interpreting mixing patterns of different soil bioturbation processes through luminescence and numerical modelling. SOIL 11, 51-66, http://doi.org/10.5194/soil-11-51-2025

Zhang, A., Long, H., Yang, F., Zhang, J., Peng, J., Gong, K., Hong, Y., Shi, Y., Zhou, S., Shao, Z., Yang, N., Huang, X., Luo, X., Zhang, G., 2025. Revisiting krotovina formation using luminescence dating − a case study from NE China. CATENA 248, 108554, http://doi.org/10.1016/j.catena.2024.108554

- rock surface burial or exposure dating

Margirier, A., Brondex, J., Rowan, A. V., Schmidt, C., Pedersen, V. K., Lehmann, B., Anderson, L. S., Veness, R., Watson, C. S., Swift, D., King, G. E., 2025. Tracking Sediment Transport Through Miage Glacier, Italy, Using a Lagrangian Approach With Luminescence Rock Surface Burial Dating of Englacial Clasts. Journal of Geophysical Research: Earth Surface 130, e2024JF007773, http://doi.org/10.1029/2024JF007773

- tephra (and volcanic related)

Yang, H., Pan, B., Chen, J., Liu, J., Liang, H., Di, N., Du, J., Li, S., 2025. Luminescence dating study of eruptions and baked sediments from Changbaishan volcano, Northeastern China. Quaternary International 724, 109738, http://doi.org/10.1016/j.quaint.2025.109738

- thermochronology

Zhang, J., Arriga, G., Rossetti, F., Argante, V., Kraemer, D., Sontag-González, M., Cosentino, D., Cipollari, P., Tsukamoto, S., 2025. Dolomite luminescence thermochronometry reconstructs the low-temperature exhumation history of carbonate rocks in the central Apennines, Italy. Communications Earth & Environment 6, 252, http://doi.org/10.1038/s43247-025-02216-1

Archaeology applications

Badino, F., Ruka, R., Pini, R., Frechen, M., Argante, V., Susini, D., Abu El Khair, D., Comolli, R., Mazzini, I., Delpiano, D., Çipa, K., Margaritora, D., Gjipali, I., Peresani, M., 2025. Palaeoenvironmental, stratigraphic and geochronological study of the coastal site of Dalani i Vogël (Vlora, Albania): new evidence for late Neanderthal occupation and prehistoric archaeology. Quaternary Science Reviews 349, 109111, http://doi.org/10.1016/j.quascirev.2024.109111

Ben Arous, E., Blinkhorn, J. A., Elliott, S., Kiahtipes, C. A., N'zi, C. D., Bateman, M. D., Duval, M., Roberts, P., Patalano, R., Blackwood, A. F., Niang, K., Kouamé, E. A., Lebato, E., Hallett, E., Cerasoni, J. N., Scott, E., Ilgner, J., Alonso Escarza, M. J., Guédé, F. Y., Scerri, E. M. L., 2025. Humans in Africa's wet tropical forests 150 thousand years ago. Nature 640, 402-407, http://doi.org/10.1038/s41586-025-08613-y

Beyin, A., Ryano, K. P., Buylaert, J.-P., Wright, D. K., 2025. Late Quaternary human occupation of the Kilwa coast (Tanzania): OSL ages and paleoenvironmental proxies from isotope geochemistry. Journal of Archaeological Science: Reports 61, 104874, http://doi.org/10.1016/j.jasrep.2024.104874

Bretzke, K., Preusser, F., Raith, K., Preston, G., Kim, S., Jasim, S., Yousif, E., Parker, A. G., 2025. Archaeology, chronology, and sedimentological context of the youngest Middle Palaeolithic assemblage from Jebel Faya, United Arab Emirates. Archaeological and Anthropological Sciences 17, 60, http://doi.org/10.1007/s12520-025-02164-z

Cleghorn, N. E., Villagran, X., Saktura, R. B. K., Jacobs, Z., 2025. Knysna Eastern Heads Cave 1 – Stratigraphy, chronology, and archaeological find density from MIS 3 to MIS 1 on the edge of the Palaeo-Agulhas Plain (south coast, South Africa). Quaternary Science Reviews 351, 109180, http://doi.org/10.1016/j.quascirev.2024.109180

Dong, Z., Hu, Z., Pan, B., Bridgland, D., Li, X., Mo, Q., Li, M., Zhong, M., Pan, R., 2025. Draining of an ancient lake in the Hexi Corridor 4500 years ago triggered migration of the Hei Shan civilization. Communications Earth & Environment 6, 403, http://doi.org/10.1038/s43247-025-02384-0

Duarte, C., Bracco Boksar, R., Gutiérrez, O., Panario, D., 2025. The mounds of the India Muerta region, Uruguay, as pit oven stations. New data. Quaternary Environments and Humans 3, 100053, http://doi.org/10.1016/j.qeh.2024.100053

Gao, Y., Zhang, D. D., Zhang, H., Zhang, S., Li, T., Chen, S., Luo, C., Cheng, H., 2025. Prehistoric human hand and footprints in Quesang on the central Tibetan Plateau from the Bølling-Allerød Interstadial. Archaeological and Anthropological Sciences 17, 71, http://doi.org/10.1007/s12520-025-02181-y

García Sanjuán, L., Rivera-Jiménez, T., Díaz-Guardamino, M., Wheatley, D., Lozano Rodríguez, J. A., Donaire Romero, T., González-García, A. C., Montero Artús, R., Ruiz Flores, J., Bermejo Meléndez, J., Rogerio-Candelera, M. Á., Ling, J., Andrieux, E., Bailiff, I., 2025. Shedding new light on the context and temporality of Iberian warrior stelae: The Cañaveral de León 2 Stela and Las Capellanías burial complex (Huelva, SW Spain). PLOS ONE 20, e0321080, http://doi.org/10.1371/journal.pone.0321080

Guo, A., Mao, L., Li, C., Mo, D., 2025. Reconstruction of the paleoenvironmental context of Holocene human behavior at the Fenghuangzui site in the Nanyang Basin, Middle Yangtze River, China. Heritage Science 13, 2, http://doi.org/10.1038/s40494-025-01631-z

Guo, X., Lu, C., Qin, Z., Dong, B., Yu, L., Bae, C. J., Sun, X., 2025. Single-grain K-feldspar pIRIR dating of the Longwanling handaxe-bearing site in the Hanjiang river valley, central China. Quaternary Science Reviews 351, 109194, http://doi.org/10.1016/j.quascirev.2025.109194

Härtling, J. W., Stele, A., Ortisi, S., Jepsen, A., Rappe, M., Bussmann, J., Fülling, A., 2025. Germanic Rampart or Roman Encampment? – New Geoarchaeological Evidence at the Roman Conflict Site at Kalkriese (NW-Germany). Geoarchaeology 40, e22031, http://doi.org/10.1002/gea.22031

Heginbotham, A., Leroy, S., Zink, A., 2025. II.8 Dating Methods. In: Bourgarit, D., Bassett, J., Bewer, F.G., Heginbotham, A., Lacey, A., Motture, P. (Eds.), Guidelines for the Technical Examination of Bronze Sculpture. J. Paul Getty Museum, Los Angeles, pp. 136–140.

Hu, G., Hu, C., Wu, X., Pan, G., Zhuma, D., He, Q., Wang, H., Wang, P., Xu, L., Xie, J., Zhang, J., Wang, X., Tang, Y., 2025. Fluvial downcutting and its influence on human settlement in the middle reaches of the Lancang River. Geomorphology 477, 109703, http://doi.org/10.1016/j.geomorph.2025.109703

Huntley, J., MacDonald, B.L., Woolgar Aboriginal Corporation, Fitzsimmons, K.E., Wallis, L.A. (2025) Assemblage first: Using provenance methods to understand 38,000 years of ochre use at Gledswood Shelter 1, Woolgar Country (northwest Queensland), Australia. Journal of Archaeological Science, 106210, http://doi.org/10.1016/j.jas.2025.106210

Jacobs, Z., Karkanas, P., Fahey, B. P., Fisher, E. C., Marean, C. W., 2025. A high-resolution chronology for the archaeological deposits at Pinnacle Point 5–6, Western Cape Province, South Africa. Quaternary Science Reviews 354, 109263, http://doi.org/10.1016/j.quascirev.2025.109263

Jacobs, Z., Zavala, E. I., Li, B., O'Gorman, K., Shunkov, M. V., Kozlikin, M. B., Derevianko, A. P., Uliyanov, V. A., Goldberg, P., Agadjanian, A. K., Vasiliev, S. K., Brink, F., Peyrégne, S., Slon, V., Pääbo, S., Kelso, J., Meyer, M., Roberts, R. G., 2025. Pleistocene chronology and history of hominins and fauna at Denisova Cave. Nature Communications 16, 4738, http://doi.org/10.1038/s41467-025-60140-6

Jin, J., Wei, J., Ling, Z., Hou, C., Xu, D., Li, Z., 2025. Optically dating of a Paleolithic site in coastal regions of South China and its correlation with the late Pleistocene environment evolution. Journal of Archaeological Science: Reports 61, 104887, http://doi.org/10.1016/j.jasrep.2024.104887

Kittel, P., Makohonienko, M., Apolinarska, K., Golyeva, A., Okupny, D., Ginter, A., Borówka, R. K., Rennwanz, J., Kramkowski, M., Poręba, G., Szymak, A., Pokutta, D., Sîrbu, G., Rybicka, M., 2025. A comprehensive palaeoecological study of humic deposits and loess profiles as a tool for understanding past human-environmental relationships at Tripolye Culture Gordineşti II-Stînca goală site, Northern Moldova. Journal of Archaeological Science: Reports 62, 105057, http://doi.org/10.1016/j.jasrep.2025.105057

Kovach, T.Z., Petrosyan, A., Wilkinson, K.N., Raczynski-Henk, Y., Rodrigues, K., Frahm, E., Beverly, E., Gill, J.P., Sherriff, J.E., Gasparyan, B. and Avetisyan, H.G., 2025. Contextualizing the Upper Paleolithic of the Armenian Highlands: New data from Solak-1, central Armenia. Journal of Human Evolution 199, 103632, http://doi.org/10.1016/j.jhevol.2024.103632

Li, Y., Gu, Y., Jiang, M., Fang, S., Fu, Z., Guan, S., Liu, R., Zhu, Z., Liu, H., 2025. Neolithic human adaptations to the environmental changes in the Jianghan Plain, middle Yangtze Valley. Quaternary Science Reviews 355, 109271, http://doi.org/10.1016/j.quascirev.2025.109271

Li, Y., Lu, P., Chen, P., Wang, H., Yang, S., Zhao, X., Liao, Y., Tian, Y., Wang, Z., Mo, D., 2025. Landform basis for the rise of early cities in the upper Jialu river basin, central China. Quaternary International 735, 109842, http://doi.org/10.1016/j.quaint.2025.109842

Magnavita, C., Lindauer, S., Adjbane, A. C., 2025. New Luminescence and Radiocarbon Dates for Kanem-Borno Fired-Brick Elite Sites in Kanem, Chad: Bayesian Chronological Modelling of Settlement Construction. African Archaeological Review 42, 1-23, http://doi.org/10.1007/s10437-025-09611-1

Malikov, D. G., Zotkina, L. V., Davydov, R. V., Malikova, E. L., Miklashevich, E. A., Petrozhitskiy, A. V., Ershova, O. V., Cherezova, A. A., 2025. Geological dating of the earliest Minusinsk Depression rock art, the Maydashy site, Southern Siberia. Quaternary Research 1-14, http://doi.org/10.1017/qua.2025.5

Möller, G. H. D., Mazel, A. D., Sommer, C., Botha, G. A., Conard, N. J., Riedesel, S., Will, M., 2025. Revisited and Revalorised: Technological and Refitting Studies at the Middle Stone Age Open-Air Knapping Site Jojosi 1 (KwaZulu-Natal, South Africa). Journal of Paleolithic Archaeology 8, 5, http://doi.org/10.1007/s41982-024-00205-y

Mukhopadhyay, S., Gupta, A., Kumar, P., Sukumaran, P., Sabale, P. D., 2025. Understanding the Microlithic technology in the Lower Ganga Basin, Eastern India: A chronological and ecological perspective. Quaternary Environments and Humans 3, 100059, http://doi.org/10.1016/j.qeh.2025.100059

Nami, H. G., Feathers, J., 2025. OSL dating on Late Pleistocene/Holocene deposits from central Uruguay, southeastern South America. Journal of Archaeological Science: Reports 62, 105036, http://doi.org/10.1016/j.jasrep.2025.105036

Oikonomou, I. A. K., Karampaglidis, T., Fenn, K., Gur-Arieh, S., Nora, D., Sánchez-Romero, L., Rogall, D. L., Vettese, D., Gasparyan, B., Petrosyan, A., Malinsky-Buller, A., 2025. Unravelling the formation processes and depositional histories of the Middle Palaeolithic Ararat-1 Cave, Armenia: A multiscalar and multiproxy geoarchaeological approach. Quaternary Science Reviews 361, 109405, http://doi.org/10.1016/j.quascirev.2025.109405

Oron, M., Avni, Y., Wieler, N., Porat, N., Sasson, E. C., Barzilai, O., 2025. Nubian Levallois Cores from MIS 5 Alluvial Terraces in the Negev Desert: New Insights into the Middle Paleolithic in the Arid Regions of the Southern Levant. Journal of Paleolithic Archaeology 8, 4, http://doi.org/10.1007/s41982-025-00208-3

Pan, Y., Zha, X., Huang, C., Pang, J., Zhou, Y., Wang, N., Zhao, Y., 2025. Vegetation change and grazing activities since the middle Holocene in the Zoige Basin, eastern Tibetan Plateau, China. Quaternary Science Reviews 357, 109330, http://doi.org/10.1016/j.quascirev.2025.109330

Rosas, A., García-Tabernero, A., Fidalgo, D., Fero Meñe, M., Ebana, C. E., Ornia, M., Fernández-Martínez, J., Sánchez-Moral, S., Morales, J. I., 2025. Middle Stone Age (MSA) in the Atlantic rainforests of Central Africa. The case of Río Campo region in Equatorial Guinea. Quaternary Science Reviews 349, 109132, http://doi.org/10.1016/j.quascirev.2024.109132

Schmidt, C., Veres, D., Murătoreanu, G., Cosac, M., Niţă, L., Vasile, Ş., Şerbănescu, G. S., Bartok, I.-E., 2025. Evidence for the oldest Middle Palaeolithic cave occupation in the Romanian Carpathians. Journal of Quaternary Science 40, 22-35, http://doi.org/10.1002/jqs.3667

Su, Y., Zhang, Y., Zhai, Q., Shi, T., Wang, S., Chen, P., Liu, X., Jin, L., Miao, X., 2025. Prehistoric archaeological site changes and their causes with paleofloods in Southern Shanxi Province, China. Quaternary Science Reviews 351, 109182, http://doi.org/10.1016/j.quascirev.2025.109182

van Beek, R., Chamberlain, E. L., de Nooijer, K., Gerritsen, S., Bartels, M., Wallinga, J., 2025. Dating earthworks with luminescence: Insights from the medieval ringfort of Den Burg, Texel (the Netherlands). Quaternary Geochronology 88, 101669, http://doi.org/10.1016/j.quageo.2025.101669

Zaidner, Y., Prévost, M., Shahack-Gross, R., Weissbrod, L., Yeshurun, R., Porat, N., Guérin, G., Mercier, N., Galy, A., Pécheyran, C., Barbotin, G., Tribolo, C., Valladas, H., White, D., Timms, R., Blockley, S., Frumkin, A., Gaitero-Santos, D., Ilani, S., Ben-Haim, S., Pedergnana, A., Pietraszek, A. V., García, P., Nicosia, C., Lagle, S., Varoner, O., Zeigen, C., Langgut, D., Crouvi, O., Borgel, S., Sarig, R., May, H., Hershkovitz, I., 2025. Evidence from Tinshemet Cave in Israel suggests behavioural uniformity across Homo groups in the Levantine mid-Middle Palaeolithic circa 130,000–80,000 years ago. Nature Human Behaviour 9, 886-901, http://doi.org/10.1038/s41562-025-02110-y

Zhou, G., Zuo, X., Zhou, Z., Jin, J., Fan, X., Wei, J., Pei, Y., Xie, H., Huang, Y., Ren, L., Lin, Y., 2025. Early Island rice farmers on the South China Coast during the 7th millennium BP. Journal of Archaeological Science 175, 106158, http://doi.org/10.1016/j.jas.2025.106158

Zink, A., Porto, E., Rante, R., 2024. Luminescence Dating of Archaeological Sites from the Oasis of Bukhara. In: The Oasis of Bukhara, Volume 3: Material Culture, Socio-Territorial Features, Archaeozoology and Archaeometry, Arts and Archaeology of the Islamic World. Brill, Leiden, pp. 382-408, http://doi.org/10.1163/978900463999_014

Zink, A., Porto, E., 2024. La datation par luminescence au C2RMF et l'archéologie [communication orale]. In : Beck, L., Bouiron, M., Carpentier, C., Cottiaux, R., Delqué-Količ, E., Féret, S. (Eds.), Datations « absolues » en archéologie : actes du 8e séminaire scientifique et technique de l'Inrap, 3-4 Dec. 2024, Orsay, http://doi.org/10.34692/pncv-k219

ESR, basic and applied research

Martins, A. A., Gouveia, M. P., Cunha, P. P., Cabral, J., Gomes, A., Falguères, C., Voinchet, P., Stokes, M., Caldeira, B., Buylaert, J.-P., Murray, A. S., Bahain, J.-J., Figueiredo, S., 2025. Marine terrace staircases of western Iberia: Uplift rate patterns from rocky limestone coasts of central Portugal (Cape Raso - Abano beach and Cape Espichel). Quaternary International 720, 109657, http://doi.org/10.1016/j.quaint.2024.109657

Obata, N., Toyoda, S., 2025. Thermal stability of the bleachable and unbleachable components of the ESR signals in sedimentary quartz. Radiation Measurements 180, 107327, http://doi.org/10.1016/j.radmeas.2024.107327

Obata, N., Toyoda, S., 2025. Thermal stability of the ESR signals of the Al and Ti-Li centers in quartz of tephra. Radiation Measurements 181, 107380, http://doi.org/10.1016/j.radmeas.2025.107380

Wang, S., Jia, Z., Xue, D., Pan, B., 2025. Temperature-dependent EPR characteristics of quartz paramagnetic centers: Some insights for dating purposes. Radiation Physics and Chemistry 229, 112469, http://doi.org/10.1016/j.radphyschem.2024.112469

Basic research

Almugren, K. S., Sabtu, S. N., Sani, S. F. A., Dzamrah, N. H., Shahira, M. N. N., Shafiqah, A. S. S., Bradley, D. A., 2025. Analysis of dosimetric properties of quartz crystals under gamma irradiation. Applied Radiation and Isotopes 218, 111699, http://doi.org/10.1016/j.apradiso.2025.111699

Amorim, Y. F., Nunes, M. C. S., Chruścińska, A., Wiśniewski, K., Trindade, N. M., 2025. First LM-OSL analysis of natural alexandrite. Radiation Measurements 184, 107441, http://doi.org/10.1016/j.radmeas.2025.107441

Ataee, N., Roberts, H. M., Duller, G. A. T., 2025. Assessing the potential of a modified post-isothermal IRSL (pIt-IR) protocol to circumvent the problems posed by anomalous fading in polymineral fine grains. Quaternary Geochronology 88, 101676, http://doi.org/10.1016/j.quageo.2025.101676

Bateman, M. D., Davies, E., Evans, D. J. A., Roberts, D. H., Connell, E. R., Rhodes, E. J., 2025. Developing a new approach to the luminescence dating of sediments from glacial contexts. Quaternary Geochronology 87, 101659, http://doi.org/10.1016/j.quageo.2025.101659

Buchanan, G., Preusser, F., Fitzsimmons, K.E., Lauer, T., 2025. Investigating the characteristics of low temperature yellow stimulated luminescence on potassium feldspar. Radiation Measurements 183, 107421, http://doi.org/10.1016/j.radmeas.2025.107421

Colarossi, D., Duller, G. A. T., Roberts, H. M., Stirling, R. J., Penkman, K. E. H., 2025. The effect of light exposure on the thermoluminescence signal from calcitic opercula. Radiation Measurements 183, 107417, http://doi.org/10.1016/j.radmeas.2025.107417

Constantin, D., Begy, R., Vandenberghe, D. A. G. J., Veres, D., Timar-Gabor, A., 2025. An empirical study on the variability of luminescence ages for coeval sediment samples. Radiation Measurements 182, 107401, http://doi.org/10.1016/j.radmeas.2025.107401

de Boer, A.-M., Steinbuch, L., Heuvelink, G.B.M., Wallinga, J., 2025. A novel method to assess crosstalk in single-grain luminescence detection. Radiation Measurements 186, 107459. http://doi.org/10.1016/j.radmeas.2025.107459

Gong, Z., Yan, H., Luo, M., 2025. Study the effect of irradiation, optical bleaching and heating on the thermal stability of OSL signals of quartz from dune sands in northern China. Quaternary Geochronology 88, 101672, http://doi.org/10.1016/j.quageo.2025.101672

Karimi Moayed, N., Fattahi, M., Autzen, M., Haghshenas, E., Tajik, V., Shoaie, Z., Bailey, M., Sohbati, R., Murray, A. S., 2024. The sensitisation of quartz extracted from andesite. Radiation Measurements 170, 107048, http://doi.org/10.1016/j.radmeas.2023.107048

Kitis, G., Polymeris, G. S., Peng, J., 2025. Determining equivalent dose for optically stimulated luminescence (OSL) dating with physically meaningful dose response curves. Quaternary Geochronology 88, 101671, http://doi.org/10.1016/j.quageo.2025.101671

Lawless, J. L., Timar-Gabor, A., 2024. A new analytical model to fit both fine and coarse grained quartz luminescence dose response curves. Radiation Measurements 170, 107045, http://doi.org/10.1016/j.radmeas.2023.107045

Mammadov, S., Gurbanov, M., Rahimli, R., Ahadova, A., Ahadov, A., Abishov, A., 2025. Analysis of thermoluminescence parameters of natural quartz: impact of thermal cleaning and irradiation doses. Journal of Radioanalytical and Nuclear Chemistry, http://doi.org/10.1007/s10967-025-10162-7

Pawlak, N. K., Chruścińska, A., 2025. Reliability of trap-filling parameters read from OSL dose-response curves measured by procedures with sensitivity correction. Radiation Physics and Chemistry 227, 112365, http://doi.org/10.1016/j.radphyschem.2024.112365

Spooner, N. A., Williams, O. M., Questiaux, D. G., 2024. Pulsed infrared stimulated luminescence measurements for defect pair model studies in feldspars. Radiation Measurements 170, 107044, http://doi.org/10.1016/j.radmeas.2023.107044

Williams, O. M., Spooner, N. A., 2025. Charge carrier release mechanisms underlying the emission of alkali feldspar infrared stimulated luminescence. Radiation Measurements 181, 107362, http://doi.org/10.1016/j.radmeas.2024.107362

Winzar, J. A., Duller, G. A. T., Roberts, H. M., Gunn, M., Bell, A. M. T., 2025. Intensity and optical resetting of Infrared Photoluminescence (IRPL) and Infrared Stimulated Luminescence (IRSL) signals in feldspars. Journal of Luminescence 278, 121018, http://doi.org/10.1016/j.jlumin.2024.121018

Xu, S., Rui, X., Guo, Y., Li, B., 2025. Testing micro-aliquot SGC and LnTn methods for age determination up to 780 ka using coarse K-feldspar grains from Nihewan Basin, northern China. Quaternary Geochronology 88, 101673, http://doi.org/10.1016/j.quageo.2025.101673

Dosimetry

Çetinkaya, H., 2025. Determination of self-attenuation correction factors for 3″×3″ NaI(Tl) detector by using Monte Carlo Code FLUKA. Radiation Physics and Chemistry 230, 112560, http://doi.org/10.1016/j.radphyschem.2025.112560

Minerals other than quartz and feldspar

Amorim, Y. F., Nunes, M. C. S., Chruścińska, A., Wiśniewski, K., Trindade, N. M., 2025. First LM-OSL analysis of natural alexandrite. Radiation Measurements 184, 107441, http://doi.org/10.1016/j.radmeas.2025.107441

Avci, H., Bulcar, K., Oglakci, M., Sayın, Ü., Topaksu, M., Atav, Ü., 2025. Thermoluminescence and electron paramagnetic resonance study on black obsidian from Mt. Ağrı. Radiation Physics and Chemistry 235, 112876, http://doi.org/10.1016/j.radphyschem.2025.112876

Biernacka, M., Majgier, R., Staninski, K., Kaczmarek, M., Zelek-Pogudz, S., Sądel, M., Szufa, K. M., Blanke, H., Kreutzer, S., 2025. The blue halite in Morsleben, Germany: A natural lyoluminescence dosimeter? Journal of Luminescence 280, 121088, http://doi.org/10.1016/j.jlumin.2025.121088

Colarossi, D., Duller, G. A. T., Roberts, H. M., Stirling, R. J., Penkman, K. E. H., 2025. The effect of light exposure on the thermoluminescence signal from calcitic opercula. Radiation Measurements 183, 107417, http://doi.org/10.1016/j.radmeas.2025.107417

Schmidt, C., Halter, T., Hanson, P. R., Ulianov, A., Putlitz, B., King, G. E., Kreutzer, S., 2024. Zircon luminescence dating revisited. Geochronology 6, 665-682, http://doi.org/10.5194/gchron-6-665-2024

Zhang, J., Arriga, G., Rossetti, F., Argante, V., Kraemer, D., Sontag-González, M., Cosentino, D., Cipollari, P., Tsukamoto, S., 2025. Dolomite luminescence thermochronometry reconstructs the low-temperature

exhumation history of carbonate rocks in the central Apennines, Italy. Communications Earth & Environment 6, 252, http://doi.org/10.1038/s43247-025-02216-1

Instruments

Çetinkaya, H., 2025. Determination of self-attenuation correction factors for 3″×3″ NaI(Tl) detector by using Monte Carlo Code FLUKA. Radiation Physics and Chemistry 230, 112560, http://doi.org/10.1016/j.radphyschem.2025.112560

Kim, H., Hwang, J., Lim, K. T., 2024. Quantitative analysis of silicon photomultipliers for thermoluminescence measurement. Radiation Measurements 175, 107172, http://doi.org/10.1016/j.radmeas.2024.107172

Richter, D., Richter, A., Kumar, T., Pintaske, R., Dornich, K., 2025. Lexsyg luminescence measurement devices: Status and outlook. Radiation Measurements 181, 107377, http://doi.org/10.1016/j.radmeas.2025.107377

Portable instruments

Nikolskaia, P., Ackermann, O., Janovský, M., Fišer, J., Anker, Y., Anker, Y., Ben-Gedalya, T., Friedman, A., Hejcman, M., Reed, K., Shai, I., 2025. Identification of the ancient anthropogenic Catena by deciphering hidden physical and chemical markers through pOSL and pXRF analysis. CATENA 250, 108708, http://doi.org/10.1016/j.catena.2025.108708

Robins, L., Roskin, J., Porat, N., Taxel, I., 2025. Punctuated landscape evolution of the Caesarea (Israel) plot-and-berm agroecosystem in coastal sand inferred from port-OSL and OSL chronologies. CATENA 250, 108735, http://doi.org/10.1016/j.catena.2025.108735

Review

Yang, J., Chen, S., Ling, Z., Zhang, C., Wang, L., Wang, H., Wang, S., Gao, F., Lizaga, I., Wang, F., Yang, S., Chen, F., 2025. Spatiotemporal evolution of aeolian sedimentary landscapes on the southern Tibetan Plateau during the late Quaternary: A review and recent advances. Earth-Science Reviews 261, 105035, http://doi.org/10.1016/j.earscirev.2024.105035

Statistics, simulation, and modelling

de Boer, A.-M., Steinbuch, L., Heuvelink, G.B.M., Wallinga, J., 2025. A novel method to assess crosstalk in single-grain luminescence detection. Radiation Measurements 186, 107459, http://doi.org/10.1016/j.radmeas.2025.107459

Pawlak, N. K., Chruścińska, A., 2025. Reliability of trap-filling parameters read from OSL dose-response curves measured by procedures with sensitivity correction. Radiation Physics and Chemistry 227, 112365, http://doi.org/10.1016/j.radphyschem.2024.112365

Touliopoulos, A., Kitis, G., 2025. Simulation of peak properties in thermoluminescence dosimeters with the potential stimulation of all electron traps. Radiation Physics and Chemistry 228, 112395, http://doi.org/10.1016/j.radphyschem.2024.112395

Conference Announcements: APLED 2025

We are delighted to announce that the 2025 APLED Conference will be held on Jeju Island, South Korea, from September 21 to 24, 2025.

The aim of this conference is to promote the exchange of research related to the development and application of luminescence and electron spin resonance methods, with a focus on their uses in solid-state physics, archaeology, geology, geomorphology, and planetary sciences. We also welcome novel and interdisciplinary contributions in emerging fields.

While the conference primarily targets the Asia-Pacific region, participants from around the world are also warmly invited to join.

The official website is now available: https://2025apled.com/

Registration and abstract submission are now open!

Important Deadlines

- Abstract Submission Deadline: July 31, 2025
- Registration Deadline: August 15, 2025

Please feel free to share this announcement with your colleagues and peers in the luminescence and ESR communities. We look forward to welcoming you to Jeju Island for an inspiring and impactful conference.

Contact us: apled2025@gmail.com

Aims and Scope
Ancient TL (electronic ISSN 2693-0935) is a community-based, not-for-profit, peer-reviewed, diamond open access journal devoted to theoretical and experimental luminescence and electron spin resonance (ESR) research. This includes research on environmental dose rate, rock thermal histories (e.g., low-temperature thermochronometry) and mineral provenance and characterisation. Manuscripts on luminescence and ESR dating, on software codes, numerical models and on instrumentation are also welcome. Ancient TL also publishes interlaboratory comparisons, standardisation procedures, failed experiments, as well as observations difficult to explain. Following Ancient TL's tradition, manuscripts about practical aspects of laboratory and field work are explicitly welcome. Periodically, Ancient TL publishes an up-to-date bibliography, thesis abstracts, and miscellaneous information for the community.

Frequency
Two issues per annum in June and December

Submission of articles to Ancient TL
For instructions to authors and information on how to submit to Ancient TL, please visit the website at:
http://ancienttl.org/TOC1.htm

Journal Enquiries
For enquiries please contact the editor:
Christoph Schmidt, Institute of Earth Surface Dynamics, University of Lausanne, 1015 Lausanne, Switzerland, Tel: +41-21-692-3516 (christoph.schmidt@unil.ch)

Subscriptions to Ancient TL
Ancient TL Vol. 32, No. 2 December 2014 was the last issue to be published in print. Past and current issues are available for download free of charge from the Ancient TL website:
http://ancienttl.org/TOC4.htm